THE ASTROPHYSICAL JOURNAL, 354:446–467, 1990 May 10

ULTRAVIOLET AND OPTICAL VARIATIONS IN ACTIVE GALACTIC NUCLEI: THE SEYFERT 1 GALAXY NGC 5548[1]

W. WAMSTEKER,[2,3] P. RODRÍGUEZ-PASCUAL,[4] BEVERLEY J. WILLS,[5] H. NETZER,[6] D. WILLS,[5] R. GILMOZZI,[3,7] M. BARYLAK,[2,3] A. TALAVERA,[2,3] D. MAOZ,[6] P. BARR,[3,8] AND A. HECK[9]

Received 1989 August 3; accepted 1989 November 15

ABSTRACT

We describe the results of a project to study the combined ultraviolet-optical spectrum of the Seyfert 1 galaxy NGC 5548 over the period 1978–1986. Of the many spectrophotometric observations made with a typical resolution of 5–8 Å, 11 epochs were simultaneous and nine cover the range from 1150 to 7000 Å. The combined *IUE* and ground-based observations, frequently obtained only a few days apart, enable us to study, for the first time, the time variability of many UV and optical lines, the overall shape of the nonstellar continuum, and the relations between the two. The variable continuum was found to be well represented by a power law, $F_\nu \propto \nu^{-\alpha}$, with α varying between 0.1 and 0.5 over 1.5 mag changes in the UV continuum. We have measured the strength of the Balmer continuum and the Fe II blends with the aid of theoretical models and found small variations in the strengths of the Fe II multiplets in the UV only, and large variations in the Balmer continuum. The detailed continuum analysis allowed us to study the line profiles and show that they are well represented by five components. The narrow (<1400 km s^{-1}) component in most lines does not vary with the continuum except for Lyα where the variations suggest a 3 year delay with respect to the continuum variations. A very broad component (10,000 km s^{-1}) is seen in all high-excitation lines, most notably in He II, while a broad (5000 km s^{-1}) component produces most of the flux in the hydrogen Balmer lines, and the low-excitation lines such as Mg II λ2798. In some lines there are also "blue" and "red" broad components. The behavior of the continuum and individual line components is studied in detail. We find among other results, that:

a) The very broad component has a blueshift of 2000 km s^{-1}, possibly indicating obscuration in the innermost parts of an accretion disk;

b) Unlike Lyα, the very broad C IV λ1549 does not continue to increase with the UV continuum at large flux levels. This may indicate a transition to C^{+4}, a matter bounded situation, or it could be a consequence of hysteresis type behavior in undersampled data.

c) For the broad component, the ratio C III] λ1909/C IV λ1549 is independent of the continuum luminosity, suggesting a large ionization parameter.

d) The Balmer decrement in the broad component is smaller when the continuum is brighter. Lyα and Hγ increase more than Hα and Hβ with the increasing UV flux.

e) The He II lines are very broad and change by a factor of up to 4. They seem to react quickly to UV continuum changes, and there is no need to invoke "accretion" events to explain their variability.

Subject headings: galaxies: individual (NGC 5548) — galaxies: nuclei — galaxies: photometry — galaxies: Seyfert — ultraviolet: spectra

I. INTRODUCTION

Monitoring of Seyfert 1 galaxies and other active galactic nuclei (AGNs) at X-ray, ultraviolet, optical, and infrared wavelengths has shown that variability on time scales of days to years is quite common for such objects (e.g., Lyutyi 1977; Collin-Souffrin, Alloin, and Andrillat 1973; Yee and Oke 1981; Alloin *et al.* 1985; Kollatschny *et al.* 1981; Peterson *et al.* 1982; Ulrich *et al.* 1984; Clavel *et al.* 1987; Barr and Mushotsky 1986; Ulrich, Courvoisier, and Wamsteker 1988; Peterson 1987*a*). These studies show continuum variability as well as changes in the strength and profile of the strong broad emission lines. The continuum and line variations are most noticeable in the ultraviolet (Wamsteker *et al.* 1985). Although variability is well established for most Seyfert 1 galaxies studied in sufficient detail, there has been little systematic monitoring of these objects. In particular, data with the extended wavelength and time coverage needed to test the relations among the various variables against theoretical models are still scarce.

Such observations are needed to understand the excitation mechanisms in AGNs. In 1982 we began a long-term project to study the ultraviolet and optical spectra of some bright Seyfert 1 galaxies. We aimed for complete coverage of the spectrum from 1100 to 7000 Å and, when possible, we obtained X-ray observations. Most of the ground-based data for this program were obtained at the McDonald Observatory of the University of Texas and the ESO Observatory at La Silla. The *IUE* data were obtained mainly under the VILSPA Observatory

[1] Based on observations made with the *International Ultraviolet Explorer* Satellite at the ESA *IUE* Observatory in Vilspa, Spain and data obtained from the *IUE* Archive.

[2] ESA *IUE* Observatory, VILSPA, Madrid, Spain.
[3] Affiliated with the Astrophysics Division, Space Sciences Department.
[4] Universidad Complutense, Madrid, Spain.
[5] Department of Astronomy, University of Texas.
[6] School of Physics and Astronomy and the Wise Observatory, Tel Aviv University, Israel.
[7] Space Telescope Science Institute.
[8] *EXOSAT* Observatory, ESA/ESTEC, Noordwijk, Holland.
[9] C.D.S., Strasbourg, France.

TABLE 1

LOG OF *IUE* SPECTRA OF NGC 5548

Image Number	Aperture[a]	FES Counts[b]	Exposure Time[c]	Julian Date (−2,440,000)	Date	Reference[d]
SWP 1862	L	72	84	3687	1978 Jun 27	1
LWR 1738	L	72	120	3687	1978 Jun 27	
	S	...	15	3687	1978 Jun 27	
LWR 4768	L	89	55	4037	1979 Jun 12	
SWP 5500	L	87	40	4037	1979 Jun 12	1
LWR 4769	L	80	35	4037	1979 Jun 12	
SWP 5687	L	99	150	4055	1979 Jun 30	1, 2
LWR 4929	L	95	60	4056	1979 Jul 1	2, 3
SWP 5688	L	95	40	4056	1979 Jul 1	1, 2, 3
SWP 5689	L	95	30	4056	1979 Jul 1	1, 2, 3
SWP 7345	L	78	195	4216	1979 Dec 8	1
LWR 6334	L	77	195	4216	1979 Dec 8	
SWP 7393	L	...	50	4221	1979 Dec 13	1
LWR 6383	L	...	90	4221	1979 Dec 13	
LWR 7464	L	70	80	4339	1980 Apr 9	2
SWP 8708	L	74	90	4339	1980 Apr 9	1, 3
SWP 8751	L	74	50	4344	1980 Apr 14	1, 4
SWP 8752	L	76	40	4344	1980 Apr 14	1
LWR 7489	L	82	30	4344	1980 Apr 14	
SWP 9379	L	63	180	4417	1980 Jun 27	1, 2, 5
LWR 8131	L	59	60	4417	1980 Jun 27	2, 5
SWP 9380	L	65?	32	4417	1980 Jun 27	1, 5
SWP 9679	L	71?	68	4454	1980 Aug 3	1, 3
SWP 10692	L	64	180	4570	1980 Nov 27	1, 4, 6
SWP 13354	L	48	63	4658	1981 Feb 24	1, 4, 6, 7
LWR 10850	L	55	60	4770	1981 Jun 14	3
SWP 14253	L	50	60	4770	1981 Jun 14	1, 3, 4, 7
SWP 14398	L	56	90	4790	1981 Jul 4	1, 4
LWR 11009	L	56	75	4790	1981 Jul 4	
SWP 15701	L	67	60	4948	1981 Dec 10	1, 4, 7
SWP 15792	L	67	60	4956	1981 Dec 18	1, 4, 7
LWR 12164	L	60	60	4956	1981 Dec 18	
SWP 15855	L	59	90	4961	1981 Dec 23	1, 4, 7
LWR 12193	L	61	80	4961	1981 Dec 23	
LWR 12490	L	61	70	5000	1982 Feb 1	
SWP 16233	L	61	86	5000	1982 Feb 1	1, 4, 7
LWR 12904	L	71	60	5060	1982 Mar 30	
SWP 16667	L	71	83	5060	1982 Mar 30	1
SWP 17445	M	75	150	5170	1982 Jul 19	1, 4, 7
LWR 13717	L	100	30	5170	1982 Jul 19	
SWP 18782	L	84	30	5316	1982 Dec 12	1
SWP 18857	L	70	30	5326	1982 Dec 22	1
SWP 18890	M	74	150	5329	1982 Dec 25	1, 4, 7
SWP 18892	L	75	60	5330	1982 Dec 26	1
LWR 14920	L	76	60	5330	1982 Dec 26	
SWP 18893	S	74	60	5330	1982 Dec 26	1
LWR 15025	L	92	60	5343	1983 Jan 9	
SWP 18976	L	78	70	5343	1983 Jan 9	1
	S	78	40	5343	1983 Jan 9	
SWP 19231	L	73	85	5373	1983 Feb 9	1
LWR 15220	L	70	85	5373	1983 Feb 9	
LWR 15912	L	102	20	5468	1983 May 12	
LWR 15949	L	73	100	5471	1983 May 15	
SWP 19990	L	72	100	5471	1983 May 15	1, 4, 7
LWR 15950	L	73	95	5471	1983 May 15	
SWP 19991	L	74	98	5471	1983 May 15	1
SWP 21761	L	70	80	5683	1983 Dec 13	1
LWP 2406	L	71	70	5683	1983 Dec 13	
SWP 21864	L	69	90	5693	1983 Dec 24	1
	S	69	14	5693	1983 Dec 24	
LWP 2726	L	65	60	5731	1984 Feb 1	
SWP 22178	L	65	90	5731	1984 Feb 1	1
LWP 2727	L	71	90	5731	1984 Feb 1	
SWP 22179	L	70	96	5731	1984 Feb 1	1
SWP 22652	M	78	130	5793	1984 Apr 2	1, 4, 7
SWP 23018	M	78	150	5835	1984 May 14	1
LWP 3365	M	74	100	5835	1984 May 14	
SWP 23065	L	80	80	5842	1984 May 21	1
LWP 3399	L	77	70	5842	1984 May 21	
SWP 23066	L	82	29	5842	1984 May 21	1

TABLE 1—*Continued*

Image Number	Aperture[a]	FES Counts[b]	Exposure Time[c]	Julian Date (−2,440,000)	Date	Reference[d]
LWR 15025.....	L	92	60	5343	1983 Jan 9	
SWP 25902.....	L	64	100	6196	1985 May 10	
LWP 5948.....	L	66	60	6196	1985 May 10	
SWP 25903.....	L	68	170	6196	1985 May 10	
LWP 7635.....	L	80	75	6466	1986 Feb 6	
SWP 27673.....	L	89	94	6466	1986 Feb 6	
SWP 28699.....	L	68	90	6629	1986 Jul 17	
LWP 8648.....	L	68	65	6629	1986 Jul 17	
SWP 28700.....	L	68	165	6629	1986 Jul 17	
LWP 8649.....	L	70	91	6629	1986 Jul 17	

[a] The *IUE* has two apertures a 10″ × 20″ oval (L) and a circular of 3″ diameter (S). M = Multiple exposure in L aperture.

[b] All FES measurements were made in the slow track/overlap mode. The data are corrected for FES sensitivity decrease (Barylak, Wasatonic, and Imhoff 1985).

[c] The exposure times are given in minutes.

[d] REFERENCES.—(1) Wamsteker and Colina 1986. (2) Veron-Cetty, Veron, and Tarenghi 1983. (3) Barr, Willis, and Wilson 1983. (4) Stoner and Ptak 1985. (5) Ulrich and Boisson 1983. (6) Gregory, Ptak, and Stoner 1982. (7) Stoner and Ptak 1984.

Program. Partial results on the Seyfert I galaxy Fairall 9 and the broad-line radio galaxy (BLRG) 3C 390.3 have been published elsewhere (Wamsteker *et al.* 1985; Clavel and Wamsteker 1987; Clavel, Wamsteker, and Glass 1989). Some observations were also coordinated with the European X-Ray satellite, *EXOSAT*.

In this paper, we present and discuss optical and ultraviolet results obtained for the Seyfert 1 galaxy NGC 5548. Preliminary results have been reported by Wamsteker *et al.* (1984, 1986) and Rodríguez-Pascal *et al.* (1988). The variability of NGC 5548 has also been studied by Peterson (1987*a*, *b*), Stirpe, Van Groningen, and de Bruyn (1988), and Netzer *et al.* (1989). In § II we describe the ground-based and UV observations. Section III describes the methods used for the detailed continuum and line decomposition and analysis. The results of the continuum and line analysis are described in detail in § IV. The main conclusions are discussed in § V. In § VI the results for NGC 5548 are summarized. The error analysis is described in the Appendix.

II. OBSERVATIONS AND REDUCTION

a) Ultraviolet Observations

The ultraviolet observations were made with the *International Ultraviolet Explorer* Satellite (*IUE*: Boggess *et al.* 1978; Faelker, Gordon, and Sandford 1987) at low resolution (FWHM 6–10 Å). Most of the UV data were taken for the specific study described here, but we have analyzed all UV spectra of NGC 5548 in the *IUE* Archives up to 1986 July. All UV data were processed with the "new" version of IUESIPS (Bohlin, Holm, and Lindler 1981) to obtain a homogeneous data set. In this IUESIPS version, the calibration of the long-wavelength (LWP) camera and the short-wavelength (SWP) camera still showed a 10% discrepancy. In view of the very low signal-to-noise ratio in the *IUE* data between 1950 and 2200 Å, this does not affect our results significantly, nor does the fact that no corrections have been applied for the variation in the sensitivity of the LWR camera with time (Clavel, Gilmozzi, and Prieto 1988). In total, we used 44 short-wavelength (1152–1950 Å) *IUE* spectra at 37 different dates and 31 long-wavelength (1950–3200 Å) *IUE* spectra at 27 dates. The detailed *IUE* observing log is given in Table 1.

b) Optical Observations

All but one of the optical spectra were obtained with the 2.7 m telescope at the McDonald Observatory of the University of Texas, using the IDS spectrograph. One large-aperture spectrum was obtained at the Wise Observatory with the 1 m telescope and a self-scanned Digicon. We used 25 optical spectra, of which 11 were obtained within 4 days of the *IUE* observations. The optical and UV spectra overlapped in the range from 1152 to 5500 Å at 8 epochs (see Fig. 1). The observing log for the optical spectra is given in Table 2. The standard procedures used for the acquisition and reduction of the optical data have been described by Wills, Netzer, and Wills (1985, hereafter WNW). To obtain complete wavelength cover-

TABLE 2

LOG OF OPTICAL SPECTRA OF NGC 5548

Date	Aperture	Comments
1979 Jun 28	3″.0 × 5″.8	Red; clear; seeing good
1980 Mar 17	3.0 × 3.9	Red; clear; seeing > 5″
1980 Jun 15	2.2 × 2.9	Blue; clear; seeing 2″–4″
1981 May 6	5.0 × 6.5	Red; clear; FWHM = 3.5 Å
1981 Jun 28	3.0 × 3.4	Red; cloudy; seeing 2″–3″
1981 Jul 3	5.0 × 6.5	Blue; cirrus; seeing < 2″
1981 Jul 6	3.3 × 6.5	Red; clear; seeing 2″
1981 Sep 3	3.9 × 4.0	Blue; humid, Moon; seeing 2″–3″
1981 Dec 23	3.4 × 4.6	Blue; cloudy; seeing 5″
1982 Jan 26	3.4 × 4.6	Blue; clear, dusty; seeing 2″–3″
1982 Feb 24[a]	3.0 × 4.0	Red; cirrus; seeing 2″
1982 Feb 28[a]	3.0 × 4.1	Blue; very cloudy; seeing 2″–3″
1982 Mar 23	2.1 × 2.4	Red; clear; seeing var. 2″
1982 Mar 23[a]	5.0 × 6.5	Red; clear; seeing 1″–2″
1982 Mar 25[a]	ø24	Wise observatory
1982 Apr 28	2.6 × 4.0	Red; cirrus; seeing 2″
1982 Jun 21	5.0 × 6.5	Blue; part cloudy; seeing 2″
1983 Jan 19	3.0 × 4.0	Red; bit cloudy; Seeing 2″–3″
1983 Feb 8	3.0 × 4.0	Red; cloudy; seeing > 3″
1983 Mar 14[b]	6.5 × 6.5	Blue; cloudy; seeing 2″–3″
1983 Mar 17[b]	6.5 × 6.5	Red; clear; seeing 4″–5″
1983 Jul 11	6.5 × 6.5	Blue; clear; seeing 1″–2″
1984 Feb 1	6.7 × 6.5	Blue; seeing good
1984 May 26	3.0 × 3.4	Blue; clear
1984 May 27	3.0 × 3.4	Red; clear; seeing 2″

[a] Optical data used for 1982 March.

[b] Optical data used for 1983 May.

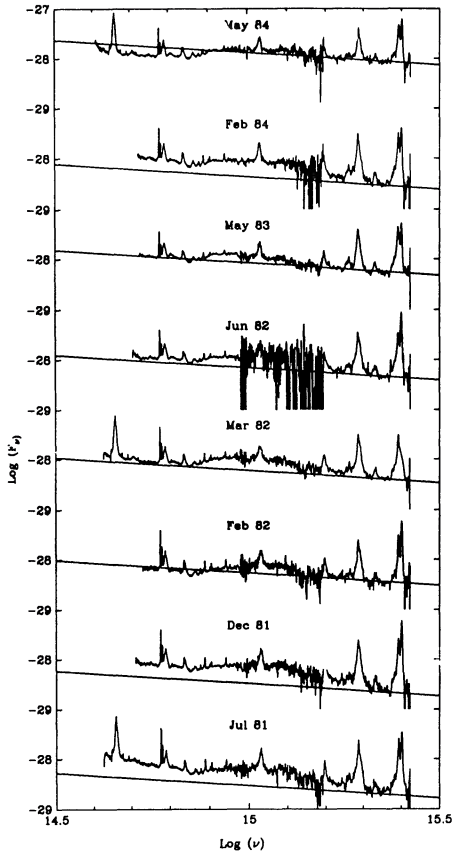

FIG. 1.—All spectra for which overlapping UV and optical data exist are shown in this figure. For the epochs 1982 March and 1983 May the time interval between the optical and UV data is larger then for the other data sets. The spectra are all on the same scale and shifted vertically with respect to each other by the same amount. The data shown are corrected for galactic reddening [$E(B-V) = 0.05$] and the redshift of NGC 5548. The thin drawn line associated with each spectrum shows a $\alpha = 0.5$ power law matched at 1350 Å for comparison. This shows the complex effects on the data of the strength of the stellar contribution with different apertures and brightness levels, as well as the influence of the small changes in the power-law slope with continuum brightness (see also Fig. 9). It is clear from this figure that it is extremely difficult to draw conclusions on the characteristics of the variable continuum on the basis of data covering a limited wavelength range.

age, the optical data were, whenever possible, taken both in the blue (3050–5200 Å) and in the red (4500–7500 Å). We also used the *IUE* Fine Error Sensor (FES) measurements (Table 1), which provide reliable photometry in a broad optical bandpass defined by the sensitivity of the FES S-20 photocathode (Holm and Rice 1981; Barylak, Wasatonic, and Imhoff 1984).

c) *Calibration and Reduction*

Here we consider data obtained within 4 days as simultaneous. Only the spectra for epochs 1982 March and 1983 May have been combined from data taken separated in time by about 30 days. In these cases, no evidence for or of significant variation between the time of the optical and UV spectra was indicated, and they can thus be treated as coeval. For convenience, all data were rebinned at 2 Å intervals, regardless of the original sampling or wavelength resolution; this does not affect the results, since it is less than $\frac{1}{3}$ of the resolution. After the standard reductions, all data were processed with the ESO-IHAP software at ESA *IUE* Observatory.

To ensure that the optical spectra are calibrated consistently and to be able to use spectra observed in nonphotometric conditions, we have normalized them using the flux in the narrow [O III] $\lambda\lambda$4959, 5007 emission lines, measured by fitting a Gaussian profile to the lines. These lines are generally found to be constant in AGNs, and our spectrophotometry obtained under photometric conditions does not show any variability. The possibility that the [O III] emitting region might be larger than the apertures normally used was checked by a comparison of the McDonald observations (Table 2) and the spectrum obtained at the Wise Observatory with an aperture area 14 times larger. These data were obtained 2 days apart under photometric conditions and were independently calibrated. The [O III] flux measurements are identical within the combined uncertainties. This indicates that the [O III] region is unresolved in the McDonald spectra, and we used the average flux value in both [O III] lines from these two spectra to calibrate all optical spectra. Our final results for the nonvariable narrow lines (Table 3) are in good agreement with those of Peterson (1987*a*) and Cohen (1983). Comparison of the UV and optical data in the overlapping wavelength range supplies an independent check on the calibrations. For a proper connection with the *IUE* data, one needs coverage to 3100 Å, but there are difficulties in calibration there caused by severe atmospheric extinction. The flux in the 3100–3200 Å region was found to be within the expected errors, although the data here are extremely noisy.

Before analysis, all data were corrected for galactic foreground reddening of $E(B-V) = 0.05$ (Burstein and Heiles 1982) with the reddening curve as parameterized by Seaton (1979), and corrected to a rest wavelength scale using a redshift $z = 0.0174$. Minor wavelength mismatches were corrected by a direct alignment of the narrow lines in the spectral interval under consideration. To illustrate the results, we show in Figure 1 all combined spectra with overlap between the optical and the ultraviolet. These have not yet been corrected for the contribution from starlight (§ III*a*). Changes of the continuum with respect to a $\alpha = 0.5$ power law ($F_\nu \propto \nu^{-\alpha}$) drawn through

TABLE 3

NARROW-LINE FLUXES

LINE	λ	FWHM (km s^{-1})	INTENSITY: This work	Peterson (1987)	Cohen (1983)	NGC 3393[a]
Lyα	1216	1480	37	...	...	25
C IV	1549	1470	20	...	...	4.8
He II	1640	1560	3.7	...	...	2.7
O III]	1663	2100	4.2	...	...	...
C III]	1909	...	4.1	...	...	1.2
Mg II	2798	860	2.0	...	...	0.8
Hγ	4341	780	0.46	0.32	0.34	0.5
[O III]	4363	810	0.94	0.58	1.07	0.2
He II	4686	760	0.33	0.29	0.25	0.3
Hβ	4861	730	1.00[b]	1.00	1.00	1.0
[O III]	4959	780	3.65	...	...	4.0
[O III]	5007	780	10.31	9.09	9.95	12.9
He I	5876	800	0.39	...	0.09	0.1
[Fe VII]	6087	700	0.56	...	0.46	0.2
[N II]	6548	570	0.48	...	...	1.6
Hα	6563	570	4.0	3.5	3.29	3.8
[N II]	6584	570	1.29	1.11	1.49	4.6

[a] Line intensities for NGC 3393 from Díaz, Prieto, and Wamsteker 1988.
[b] $F(\mathrm{H}\beta) = (5.2 \pm 0.36) \times 10^{14}$ ergs cm^{-2} s^{-1}.

the spectrum at 1350 Å are easily discernible; these changes result from real variations in the nonstellar continuum and the use of different aperture sizes.

III. LINE AND CONTINUUM MEASUREMENTS

Given the availability of simultaneous calibrated UV and optical spectra of NGC 5548, we have the opportunity to make a detailed spectral decomposition of the continuum of this object. Such an analysis is not only of interest in itself but is also needed for the detailed analysis of the emission lines (§ III*d*). As shown by WNW, the presence of a large number of blended broad permitted Fe II lines gives rise to a pseudocontinuum, with structure on a scale of the line width. The correction for many Fe II blends and the choice of the continuum slope is complex and can significantly affect the strengths and profiles of some emission lines, even for Hβ. An example of this is the suggested presence of broad wings in the [O III] lines in various galaxies by van Groningen and de Bruyn (1988) and Stirpe, van Groningen, and de Bruyn (1988), while the analysis by Wamsteker *et al.* (1985) and the results presented here, do not support the existence of such broad wings in any of the AGNs studied.

The analysis of the continua and broad lines of AGNs is complicated by the absence of a good theoretical model for the continuum spectrum. We have used a minimum component approach, i.e., restricted the continuum components as much as possible to those associated with known constituents in the central regions of active galaxies:

1. Stellar flux from the central parts of the galaxy.
2. Balmer continuum emission (Bac) from the broad-line region (BLR) gas.
3. Fe II emission from the BLR, treated here as a pseudocontinuum.
4. A relatively flat, highly variable continuum that carries most of the energy. We found this component to be well approximated by a power law ($F_\nu \propto \nu^{-\alpha}$) over the range from 1150 to 7000 Å, with α varying between 0.1 and 0.5. The existence of such a power-law spectrum is indicated by the shape of the difference between spectra at different brightness levels.

These four components describe the overall continuum of NGC 5548 quite well, as will be seen below. Studies by others (WNW; Netzer *et al.* 1985; Gilmozzi *et al.* 1986) have shown that such a description appears valid for many low- and high-luminosity AGNs. We describe the decomposition procedure below. All discussion on the AGN of NGC 5548 below is based on the data after substraction of the stellar contribution as described in § III*a* below.

a) The Stellar Contribution

The small-aperture observation in 1982 March (Table 2) was made at one of the times when the variable nonstellar continuum was brightest, so the relative galaxy contribution was very small. Because of the problems in calibrating small-aperture spectrophotometry, we were careful to observe the nearby standard star, Feige 92, at almost the same low air mass (1.04) and close in time, with the same aperture. Comparison of the data for standard stars and the galaxy with small and large apertures suggests that the small-aperture calibration is accurate to within 5% over the wavelength range of this observation (3850–6850 Å). We fitted a single power law to the UV and optical data of this epoch such that it had the smallest spectral index without being brighter than the data anywhere between 1350 and 7000 Å. Such a power-law continuum falls clearly below the observed spectrum at all wavelengths greater than 4500 Å, and we assume that the excess energy is due to starlight. To obtain a better defined stellar spectrum, the faintest spectrum with combined data (1981 July) for which we observed the same spectral slope in the UV was matched with a power law with the same slope. The flux excess over the fitted power law in this spectrum is very similar to that of an M31 type stellar continuum (Sargent, private communication). Figure 2 shows the comparison between the M31 spectrum and the stellar spectrum for NGC 5548 as derived from the difference between the large-aperture spectrum from the Wise Observatory and the nearly simultaneous intermediate-aperture McDonald observations. The spectra are well matched. We choose to use the noiseless M31 spectrum for the subtraction, rather than the observed one, which would have introduced additional noise into the data. This stellar contribution is used at all other epochs, scaled according to aperture area. This assumes a uniform distribution of stellar emission of the galaxy within the aperture (the central 2″–7″ of NGC 5548). For the data used here, such approximation is valid, since for most optical spectra used, the aperture was less than twice the seeing (Table 2). In this case, the actual brightness distribution has only very minor influence. The galaxy contribution is indicated in Table 4. Comparing our determination of the galaxy contribution with the Gunn v and i photometry on 1982 March 7 given by Malkan and Fillipenko (1983), we find 3.8 mJy at 4000 Å and 11.0 mJy at 7900 Å (uncorrected for reddening and redshift), compared with their measurements of 4.7 and 11.2 mJy, respectively. Considering the completely different methods used, the agreement is good, and we are confident that the galaxy contribution has been properly removed. The only remaining problem is the removal of some absorption lines, since the resolution of our model spectrum is considerably worse than that of our data. In principle, this could

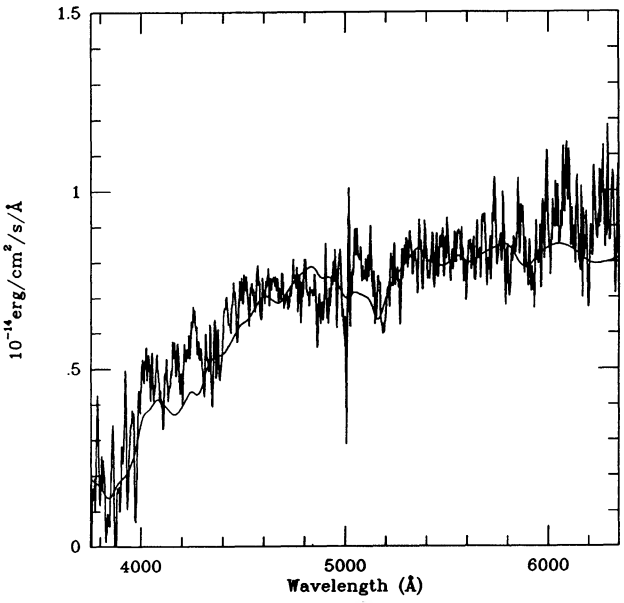

FIG. 2.—Comparison of the observed stellar spectrum in the central parts of NGC 5548 as determined from spectra with different apertures, with the M31 template used for the stellar continuum contribution, drawn as a thin line. It can be seen that even though the resolution in the template is less than in our data, the overall match is very good.

TABLE 4

OVERALL SPECTRAL CHARACTERISTICS[a]

Epoch[b]	Slope[c]	$F(1350)$	$F(5500)$	Ba-continuum	Fe II (total)	F(star)[d]	Aperture
1979 Jun	-0.45 ± 0.70	6.48 ± 0.70	0.68 ± 0.02	1221	1020	0.23	0.81
1980 Jun[e]	-0.50	8.28 ± 1.17	...	1390	955	...	0.30
1981 Jul	-0.50 ± 0.29	3.65 ± 0.43	0.50 ± 0.03	594	830	0.28	1.00
1981 Dec	-0.65 ± 0.26	4.12 ± 0.46	0.60 ± 0.05	862	990	0.20	0.73
1982 Feb	-0.25 ± 0.23	5.62 ± 0.44	0.47 ± 0.03	784	976	0.20	0.73
1982 Mar	-0.45 ± 0.17	6.87 ± 0.22	0.83 ± 0.01	1308	955	0.16	0.56
1982 Jun	-0.20 ± 0.15	7.47 ± 0.44	0.67 ± 0.02	1554	1239	0.43	1.52
1983 Jan[e]	-0.35 ± 0.18	9.05 ± 0.80	0.91 ± 0.02	1764	1037	0.16	0.56
1983 Feb[e]	-0.55 ± 0.18	6.75 ± 0.58	0.91 ± 0.02	1308	1112	0.16	0.56
1983 Apr	-0.30 ± 0.19	9.15 ± 0.60	0.62 ± 0.03	1832	750	0.55	1.97
1984 Feb	-0.40 ± 0.25	5.17 ± 0.37	0.48 ± 0.04	1143	1099	0.57	2.03
1984 May	-0.10 ± 0.14	13.89 ± 0.90	1.03 ± 0.02	1335	1588	0.13	0.48

[a] The units for the fluxes are: 10^{-14} ergs s^{-1} cm^{-2} Å^{-1}; for the Ba-continuum and Fe II, the unit is: 10^{-14} ergs s^{-1} cm^{-2}.

[b] These epochs refer to the data in Tables 1 and 2 for which the optical and UV data were taken sufficiently close in time to be treated as simultaneous.

[c] The spectral slope index (α) is defined as $F_\nu \propto \nu^\alpha$.

[d] The starlight contribution as subtracted from the data to obtain the nonthermal spectrum alone. For details see text. The aperture scaling factors are given in the last column of this table.

[e] Epochs for which no overlapping spectra were available.

affect the emission-line analysis, but such effects will be unimportant because of the spectrum-differencing method used.

b) *The Nonstellar Continuum*

Like other AGNs (e.g., Fairall 9; Clavel, Wamsteker, and Glass 1989), NGC 5548 shows a strong nonstellar continuum that seems to vary without much change in slope. We fit a single power law to the *galaxy-subtracted* data using a 40 Å wide "line-free" continuum window centered at 1350 Å. The slope is determined to be that of the flattest spectrum that is not brighter than the data at any wavelength between 1200 and 7000 Å. The spectral indices derived for the different epochs and their errors are listed in Table 4, together with the 1350 and 5500 Å nonstellar flux densities and the stellar contribution subtracted from each spectrum.

c) *Broad Emission Features:* Fe II *Lines and the Balmer Continuum*

Subtraction of the galaxy component and the best-fit power-law continuum leaves the contribution from broad and narrow emission lines as shown in Figures 3*a*–3*d* (center panels). These include isolated lines as well as broad blends of numerous Fe II lines and the Balmer continuum emission. As shown by WNW and Netzer *et al.* (1985), even though there are large uncertainties in the details of the actual physical conditions, these broad blends cannot be measured without some theoretical knowledge of the expected flux in these features, and we follow their empirical approach below.

Observationally, the Balmer continuum spectrum is constrained by the excess flux density near 3646 Å and the short-wavelength end near 1400 Å, where the models fall to zero. Fortunately, these regions are relatively free of Fe II emission lines (Fig. 3). The shape and intensity are related to the electron temperature and the Balmer edge optical depth, $\tau(3646)$, both weighted over the broad-line region. These parameters cannot easily be separated observationally, since a low T_e, large $\tau(3646)$ continuum is similar to that with a large T_e and small $\tau(3646)$. Because we are mainly interested in the fitting of the Balmer continuum flux distribution and total intensity, we choose one Balmer continuum model ($T_e = 1.4 \times 10^4$ K; $\tau(3646) = 2.0$) from WNW that gives a good fit (Fig. 3). Having fixed a model spectrum, the total Balmer continuum flux at each epoch is determined by scaling it to match the observed flux density above the power-law continuum at 3646 Å. The total Balmer continuum intensity is given in Table 4 for those epochs with overlapping data.

The flux in the broad Fe II blends was determined empirically by fitting synthetic spectra as described in WNW. Our purpose is to obtain the best line measurements possible, i.e., to remove the Fe II blends optimally from the spectrum, not to produce a theoretical model. The match to the spectrum was therefore obtained with the best fitting model, even though the physical conditions chosen for the Fe II [τ(Fe II UV) = 25; $v = 10$ km s^{-1}] and the Balmer continuum were not the same. This approach seems best, considering the uncertainties associated with modeling of AGN broad-line clouds and the general "Fe II problem" discussed by WNW. Synthetic Fe II spectra were derived from a grid of WNW models covering a large range in τ(Fe II UV) and $\tau(3646)$, the most important parameters determining the relative strengths of the different Fe II multiplets. Comparing some relatively isolated features, we found that the best match to the data was obtained for a FWHM of 4500 km s^{-1}. This is very close to the FWHM for the Hβ broad line, 4210 km s^{-1}, determined independently (Table 6). Although we treat the Fe II pseudocontinuum as a single component, the physics in the emission of different multiplets is not the same. To allow partially for this, we scaled the model to obtain a best fit in each of the three windows: Fe II(UV): 1456–2998 Å, Fe II(32): 3004–3508 Å, and Fe II(opt): 3504–6882 Å. The total Fe II fluxes are given in Table 4, while Table 5 gives the results for these three separate regions.

Figure 3 demonstrates the fit to the continuum of NGC 5548 with the stellar continuum already subtracted. The features remaining are the narrow and broad discrete emission lines, and emission between 3640 and 3900 Å, representing the merged higher order Balmer lines.

d) *Emission Lines*

For comparison with previously published data, we have measured the total line intensities by integrating over the

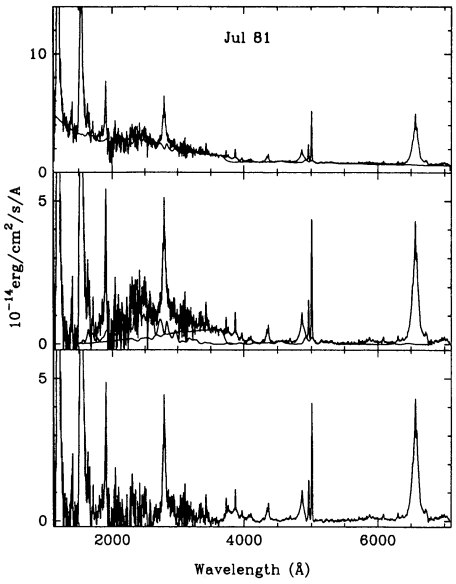

FIG. 3*a*

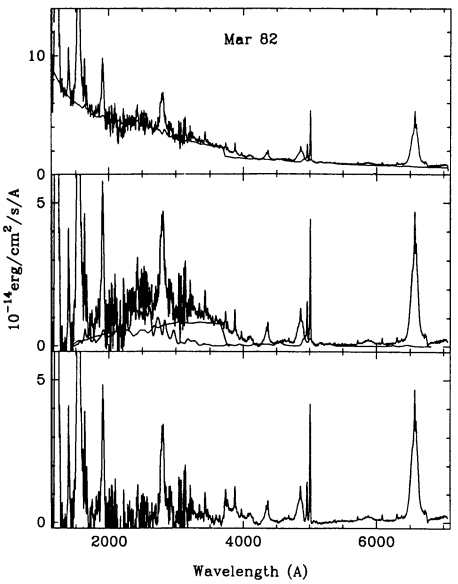

FIG. 3*b*

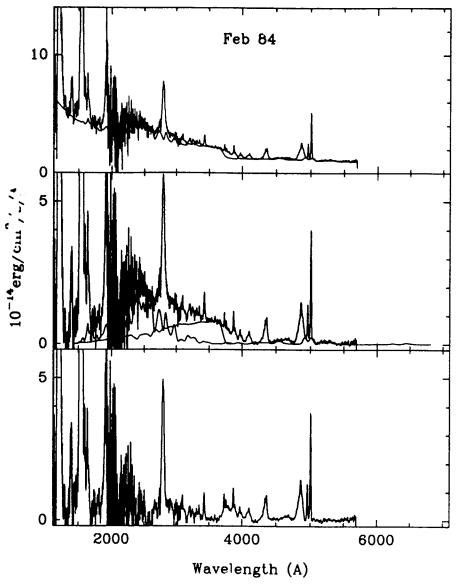

FIG. 3*c*

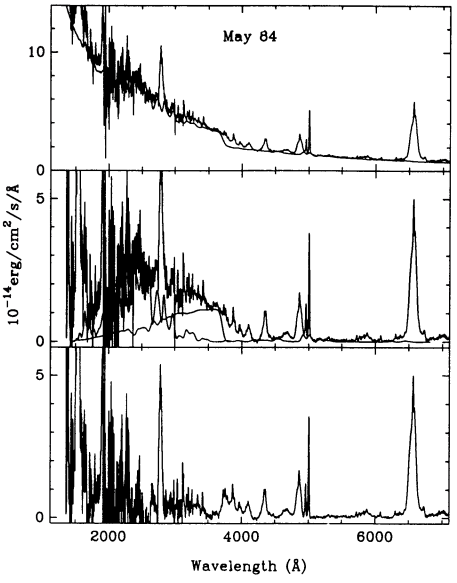

FIG. 3*d*

FIG. 3.—(*a*), (*b*), (*c*), (*d*) illustrate the continuum decomposition applied in this paper to spectra of NGC 5548 for which overlapping UV and optical data were available. The top frame shows the observed spectrum after subtraction of the contribution by the starlight in the central parts of NGC 5548. This represents the pure AGN spectrum. The complete continuum decomposition model (power-law, Balmer continuum, and Fe II pseudocontinuum) is shown as a thin continuous line in the top frame. It is obvious that with these components an excellent fit to the data from 1150 to 7000 Å is obtained, and no excess flux appears in the long-wavelength end to justify a steep power-law extension from the infrared. The sharp unmatched rise at 3646 Å corresponds to the blending of the higher Balmer lines. This has not been modeled, but can be easily accounted for. The middle frame of these figures shows the spectrum after the variable power law has been subtracted and shows the individual Fe II pseudocontinuum and the Balmer continuum. It is quite clear that the determination of the Balmer continuum is independent of the strength of the Fe II blends. The bottom frames show the pure emission-line spectrum left after the subtraction of all the continuum. The detailed line analysis was made on these data. The determination of the "standard model," using differences, was made by subtracting spectra at different epochs as shown in the top frames. The different figures (*a*), (*b*), (*c*), and (*d*) show clearly the effects of the variable continuum on all aspects of the AGN spectrum. Note the good connection between the optical and ultraviolet data at 3100 Å and the difference in the strength of the Fe II(UV) between (*a*) and (*d*), illustrating the variability of Fe II(UV) in contrast to the Fe II blends at $\lambda > 3000$ Å, for which no variability could be detected.

whole profile after continuum subtraction. The Lyα strength was measured assuming that the red side (1215–1250 Å) of the profile provides half the total line intensity. These results are given in Table 5 together with the intensity of the Balmer continuum and the Fe II blends in three separate windows. The narrow-line intensities, as derived from the final line fits, are given in Table 3.

Many studies of the broad emission lines in AGNs have centered on the analysis of line profiles, overall line shape, and line ratios as a function of velocity (e.g., Wilkes and Carswell 1982). Recent work (e.g., Wamsteker *et al.* 1985) showed that, although an increase in resolution does not allow the discrimination of separate components (e.g., Atwood, Baldwin, and Carswell 1982 for Mrk 509), one can use variability as a tool to

TABLE 5

INTEGRATED LINE INTENSITIES[a]

Line	1979 Jun	1980 Jun	1981 Jul	1981 Dec	1982 Feb	1982 Mar	1982 Jun	1983 Jan	1983 Feb	1983 May	1984 Feb	1984 May	Mean	NGC 4151
Lyα 1216[b]	1714	1938	956	1240	1146	1554	2100	2436	1839	1819	1736	1958	1692 ± 440	2314
N v λ1240	121	218	83	109	76	153	230	274	230	127	166	163	166 ± 66	...
Si IV λ1397	103	133	39	72	63	89	137	140	93	136	94	125	99 ± 33	...
C IV λ1549	1017	1415	839	1017	844	1149	1386	1468	1091	1367	1127	1239	1145 ± 216	1737
He II λ1640	58	197	74	64	64	94	109	152	82	175	110	122	102 ± 43	105
C III] λ1909	151	...	116	158	146	175	119	161	139	195	208	234	161 ± 37	217
Mg II λ2798	202	...	203	186	194	215	237	192	234	214	165	252	208 ± 27	159
Hγ	41	62	25	35	30	38	53	...	51	62	44	60	44 ± 12	...
He II λ4686	15	44	12	10	7	18	30	21	31	31	14	28	21 ± 11	13
Hβ	101	137	62	80	74	90	119	111	124	93	91	113	100 ± 23	100
[O III] λ4960	22	22	22	23	24	23	24	21	22	20	21	20	22 ± 1	...
[O III] λ5007	56	56	56	55	56	56	55	55	55	54	58	53	56 ± 1	229
He I λ5875	31	...	23	...	...	33	...	46	39	...	31	...	34 ± 8	11
Hα	483	...	392	...	...	460	...	575	526	...	483	...	486 ± 62	391
[S II] λλ6717–6731	16	...	15	...	...	16	...	21	16	...	15	...	...	...
Bac	1221	1390	594	862	784	1308	1554	1764	1308	1717	1832	1143	1251 ± 391	...
Fe II UV[c]	852	786	683	818	820	786	1154	1024	874	1229	935	1111	895 ± 146	...
Fe II 32[d]	57	53	46	55	55	53	66	59	59	115	63	74	58 ± 7	...
Fe II opt[e]	101	116	101	117	101	116	185	101	179	101	101	96	119 ± 32	...

[a] The units for fluxes are 10^{-14} ergs s^{-1} cm^{-2}.

[b] The Lyα fluxes given are measured only over half the profile; the numbers in the table are multiplied by a factor of 2. This procedure does not introduce much uncertainty since Lyα is quite symmetric (see Table 6).

[c] Fe II UV = 1456–2998 Å.

[d] Fe II 32 = 3004–3508 Å.

[e] Fe II opt = 3504–6882 Å.

isolate individual line components. A multicomponent analysis provides a useful description of line profile variations in AGNs as illustrated by a comparison of the Hβ profile of Ark 120 in 1976 and later years (Foltz *et al.* 1981), for NGC 5548 by Peterson (1987), and for Fairall 9 by Wamsteker *et al.* (1985). The separation of individual line components is difficult because the only practical method is to decompose the observed profiles into some simple analytical forms such as Gaussians (e.g., Pelat, Allain, and Fosbury 1981; Clavel *et al.* 1987). Such decomposition is nonunique when applied in a purely statistical way and is limited by insufficient resolution and signal-to-noise ratio in most *IUE* data. Clavel *et al.* (1987) used the extensive UV data set for NGC 4151 for a χ^2 analysis of the C IV λ1549 line profiles, but their analysis does not identify the same components in other lines.

For NGC 5548, we have formed *difference spectra* from the combined optical and UV data at different epochs to isolate individual components, which were represented by Gaussians, in all strong broad emission lines. The optical data with their superior signal-to-noise ratios and better velocity resolution serve as a guide for the UV data. Since Hβ and C IV λ1549 are the lines with the best signal-to-noise ratio and are available at most epochs, we have used them for the definition of *standard components* contributing to the broad-line profiles (bottom of Table 6). The standard components are:

1. A narrow component, FWHM < 1400 km s^{-1},
2. A broad component (B), FWHM = 5000 km s^{-1}, with the same systemic velocity as the narrow component,
3. A red component, FWHM = 1500 km s^{-1}, shifted by +2000 km s^{-1} with respect to the narrow lines, and
4. A blue component, FWHM = 2500 km s^{-1}, shifted by −2000 km s^{-1} with respect to the narrow lines.

In addition to these four components, we need:

5. A very broad component (VB), FWHM = 10,000 km s^{-1}, shifted to short wavelengths by 2000 km s^{-1} with respect to the narrow lines. This line was needed to account for the total C IV λ1549 profile and can be clearly seen in the difference spectra of He II λ4686 (see Fig. 4).

The panels in Figure 4 show several examples of difference spectra and demonstrate the components chosen and the usefulness of this method when enough data are available. Although Figure 4 shows most components in relatively clean form, the differences are often more complex. Nevertheless, no more than the above five components are needed to fit the profiles of all broad lines at all epochs, although not all components are present in all lines. The difference spectra in the top frames of Figure 4 show the main 5000 km s^{-1} broad component, which carries most of the variable flux for C IV λ1549 as well as for most (but not all) other lines. The lower frames in Figure 4 show the blue and red components in Hβ and the presence of the blue component only, in C IV λ1549. These differences cannot be accounted for by the normal broad line alone. Note the large variation in the very broad He II λ4686 line, confirming the need for the very broad line in the standard components. Figure 5 shows detailed overall line fits for C IV λ1549, Hβ, and Lyα. We show the line components and the residuals of the fit. The variations in the line profiles are also obvious. For Lyα, we show in Figure 5 only the part of the data used in the line fitting. Recent independent optical data (Stirpe, van Groningen, and de Bruyn 1988; Peterson 1987) confirm the existence of most of these components and their persistence over time.

The actual line fitting to the continuum-subtracted spectra was done in two steps. First χ^2 was minimized varying only the intensity of the standard components. After these fits had converged and created a reasonable representation of the line, the other fitting parameters were released for all components, first the line position and subsequently the line width (FWHM). This procedure serves to assure that the freezing of the FWHM and the line center will not cause the fitting procedure to con-

TABLE 6

LINE PROFILE DECOMPOSITION

	LINE COMPONENT FITS										
	NARROW		BROAD		VERY BROAD		RED		BLUE		
LINE	Velocity Shift	FWHM (km s^{-1})	Velocity Shift	FWHM (km s^{-1})	Velocity Shift	FWHM (km s^{-1})	Velocity Shift	FWHM (km s^{-1})	Velocity Shift	FWHM (km s^{-1})	ADDITIONAL LINES[a]
Lyα λ1216	0	1480 ± 160	−400 ± 250	5360 ± 340	−2220 ± 500	10360 ± 490	...	...	...	...	N v λ1240 Å: 2340 ± 370
C iv λ1549	0	1470 ± 130	0 ± 16	5080 ± 200	−1920	10800	...	...	−2900 ± 600	2200 ± 500	1614 Å: 4700 ± 1100
He ii λ1640	0	1560	...	...	−440 ± 420	10740	...	...	...	...	1662 Å: 2100 ± 680
C iii] λ1909	0	1420 ± 140	−260 ± 460	5130 ± 460	...	...	...	...	...	...	1895 Å: 1700 ± 550 1877 Å: 1930 ± 510
Mg ii λ2798	0	860 ± 170	200 ± 600	5250 ± 100	...	...	2080 ± 860	1270 ± 370	−1490 ± 960	1450 ± 330	...
Hγ λ4341	0	780 ± 140	−290 ± 170	4290 ± 350	...	...	2400 ± 450	2050 ± 310	−3540 ± 490	2400 ± 670	...
He ii λ4686	0	758 ± 125	...	...	−1470	8820	...	...	...	...	4628 Å: 1100 ± 220 4754 Å: 3000 ± 170
Hβ λ4861	0	730 ± 110	−260 ± 40	4210 ± 160	...	...	1740 ± 250	1730 ± 360	−3300 ± 380	2330 ± 390	4780 Å: 1000 ± 300
He i λ5875	0	800 ± 80	...	...	180 ± 40	9640	...	...	...	...	6087 Å: 690 ± 60
Hα λ6563	0	570 ± 50	96 ± 23	4690 ± 190	...	...	1920 ± 210	2070 ± 140	−2700 ± 170	2730 ± 550	6447 Å: 1200
Standard Profile	0	1000	−130	5000	−2000	10000	2000	1500	−2800	2500	...

[a] Lines that overlap with the main lines under consideration; FWHM (in km s^{-1}) and central wavelength (in Å) given. See text for discussion.

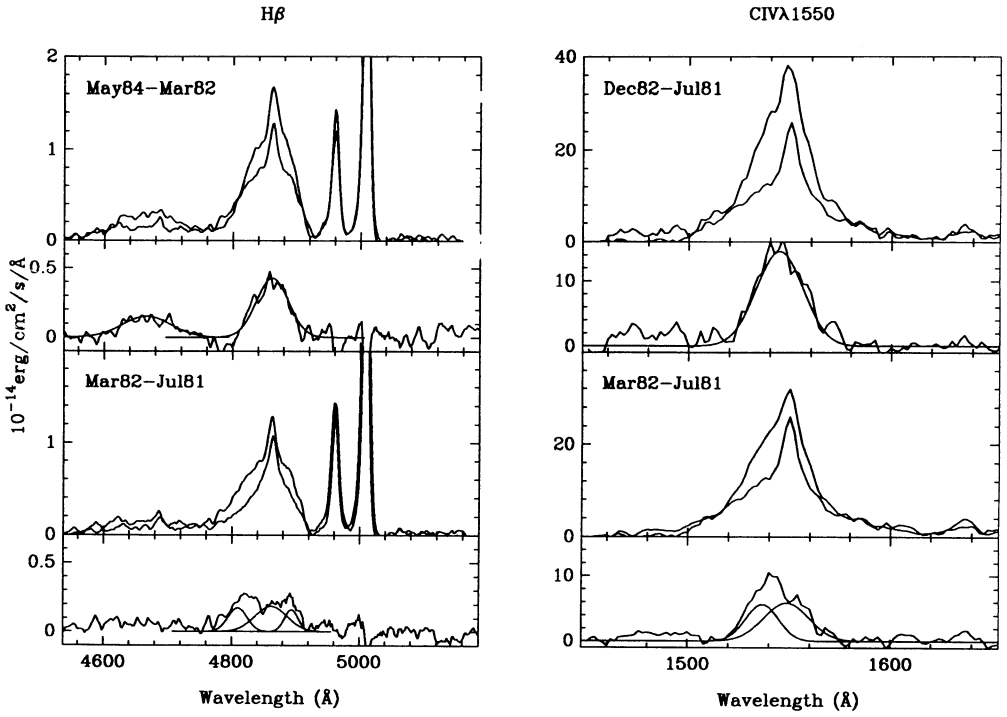

FIG. 4.—This figure illustrates the process described in § III*d* to derive the standard components used in the line decomposition of Table 6. Each top frame shows the observed lines at two epochs for C IV λ1549 to the right and Hβ on the left side (epochs indicated in the frame). Immediately below, the difference between the two profiles is shown. The top two frames show the B component (FWHM = 5000 km s^{-1}). Note also the VB variation seen in He II λ4686 on the short-wavelength side of Hβ. The frames at the bottom illustrate the red and blue components (see also Table 6), with the red component absent in C IV λ1549.

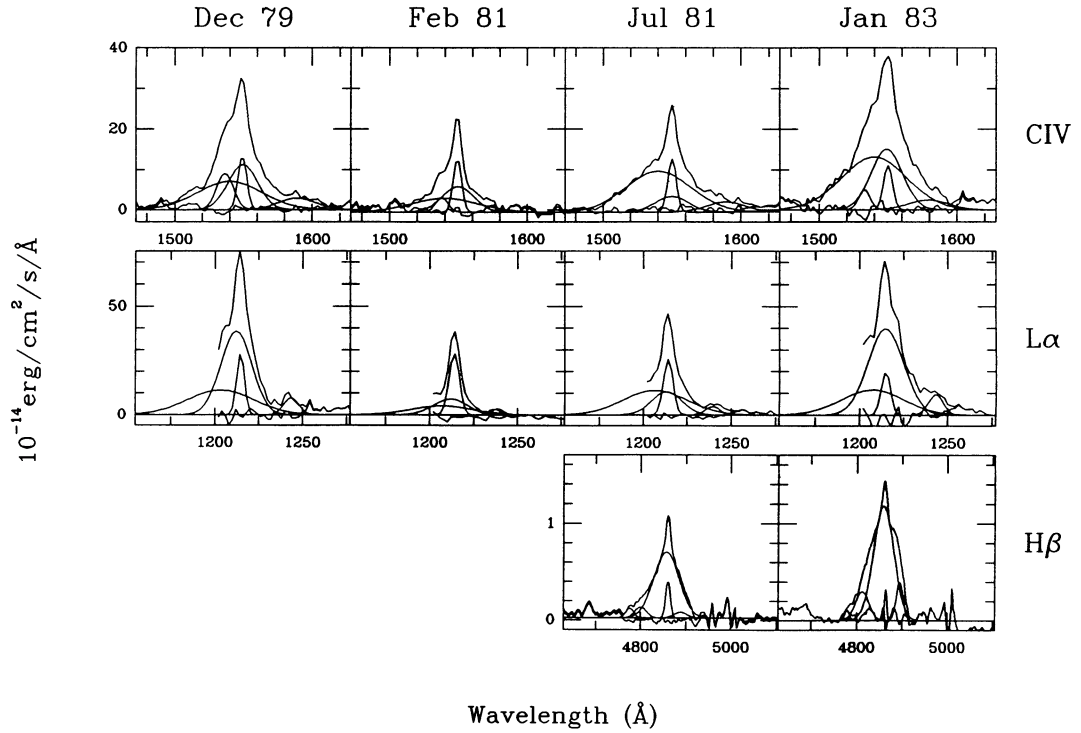

FIG. 5.—Examples of the line fits made to C IV λ1549 (*top*), Lyα (*middle*), and Hβ (*bottom*). Note that the geocoronal Lyα line has not been included in the fitting. For Lα, the fit was based on the data longward of that. For each line, we show the observed profile, the individual components as defined from the standard components in Table 6, and the residuals of the total line fit. This figure illustrates essentially all the characteristics of the lines as discussed in the text, such as the absence of a VB component in Hβ, the variation of the narrow Lyα, the variability of the red and blue components when present, and the apparent decrease in the C IV λ1549 (VB) when the continuum is very bright (see 1979 December and 1983 January).

verge to a condition that is unstable in any of these two fixed parameters; i.e., it converges to a local minimum in the χ^2 plane. Through this two-step process, we assure that the final fits start from the standard components with realistic values for the intensities. The second iteration, *final fitting*, with all line parameters free, assures a mathematically correct procedure.

Table 6 gives the derived FWHM and the average central line velocity with respect to the narrow line, with their rms errors, for all strong lines at all epochs when these could be determined. The results clearly show that for Lyα, C IV λ1549, C III] λ1909, Mg II λ2798, Hγ, Hβ, and Hα, the average values of the line positions and widths are fully consistent with the standard components, although not all components are present in all lines.

We have not only been able to fit the above-mentioned strong lines with the five component standard profile (including the narrow line) at the 11 epochs for which simultaneous data exist, but also for all other epochs when only partial data—either UV or optical—were available. For the epochs when only UV data were available, the continuum was derived using results from the epochs with full coverage (§§ IV*a* and IV*b*). This allowed us to decompose the lines for all UV data.

The component intensities for all strong lines and at all epochs are given in Tables 7–12, together with $F(1350)$. We also include measurements of N V λ1240, O III] λ1663, and some additional lines.

These lines were included in the line fits, since they overlap with the main lines under consideration. Table 6 also gives the FWHM in km s^{-1} and central wavelength in Å for most of these.

TABLE 7

LYMAN-ALPHA COMPONENTS[a]

JD	$F(1350)$	Narrow	Broad	Very Broad	NV
3686....	7.137 ± 1.165	174 ± 7	727 ± 21	633 ± 80	82 ± 42
4036....	10.931 ± 2.322	159 ± 9	764 ± 24	365 ± 270	90 ± 43
4054....	6.482 ± 0.702	129 ± 10	697 ± 19	455 ± 130	36 ± 65
4215....	10.223 ± 0.557	139 ± 12	906 ± 26	529 ± 184	78 ± 88
4220....	12.395 ± 1.389	157 ± 9	845 ± 26	541 ± 187	85 ± 60
4340....	9.469 ± 1.327	185 ± 13	605 ± 39	524 ± 173	109 ± 50
4415....	7.677 ± 1.173	168 ± 9	741 ± 45	533 ± 179	110 ± 52
4454....	4.781 ± 0.901	185 ± 6	420 ± 42	377 ± 133	54 ± 56
4570....	4.357 ± 0.338	198 ± 3	401 ± 15	388 ± 52	72 ± 34
4659....	2.626 ± 1.566	206 ± 2	177 ± 19	184 ± 60	25 ± 17
4770....	3.469 ± 0.620	175 ± 6	174 ± 52	518 ± 75	30 ± 38
4789....	3.649 ± 0.431	172 ± 5	232 ± 38	518 ± 76	42 ± 49
4949....	5.267 ± 0.856	149 ± 8	471 ± 29	411 ± 108	60 ± 33
4958....	4.120 ± 0.465	146 ± 7	390 ± 39	430 ± 102	60 ± 49
5001....	5.619 ± 0.443	170 ± 5	387 ± 33	375 ± 105	39 ± 70
5057....	6.867 ± 0.220	173 ± 7	536 ± 34	428 ± 137	60 ± 47
5169....	7.472 ± 0.436	133 ± 13	758 ± 30	454 ± 163	90 ± 46
5316....	9.613 ± 1.119	178 ± 14	869 ± 50	759 ± 196	77 ± 48
5326....	6.710 ± 0.910	146 ± 18	699 ± 39	581 ± 169	98 ± 69
5329....	8.321 ± 0.336	138 ± 10	705 ± 24	675 ± 108	82 ± 61
5330....	8.477 ± 0.403	217 ± 13	628 ± 40	775 ± 145	102 ± 63
5342....	9.053 ± 0.804	130 ± 22	967 ± 45	519 ± 266	102 ± 76
5373....	6.747 ± 0.585	145 ± 9	609 ± 22	441 ± 144	79 ± 36
5469....	9.146 ± 0.601	171 ± 8	1025 ± 24	429 ± 190	86 ± 52
5681....	8.925 ± 0.862	143 ± 9	557 ± 27	557 ± 126	54 ± 58
5692....	8.613 ± 0.555	160 ± 16	759 ± 41	490 ± 250	78 ± 62
5731....	5.173 ± 0.373	127 ± 5	689 ± 18	283 ± 174	89 ± 31
5840....	13.889 ± 0.903	173 ± 19	847 ± 43	642 ± 231	102 ± 79
6195....	3.525 ± 0.216	111 ± 4	279 ± 17	494 ± 35	35 ± 46
6467....	6.788 ± 0.499	75 ± 7	659 ± 17	398 ± 96	82 ± 43
6628....	4.016 ± 0.214	71 ± 4	232 ± 25	422 ± 47	45 ± 40

[a] $F(1350)$ is in units of 10^{-14} ergs s^{-1} cm^{-2} Å^{-1}, and the intensity of the line components is in 10^{-14} ergs s^{-1} cm^{-2}.

TABLE 8

C IV λ1549 COMPONENTS[a]

JD	$F(1350)$	Narrow	Broad	Very Broad	Blue
3686....	7.14 ± 1.16	108 ± 12	482 ± 30	511 ± 137	109 ± 32
4036....	10.93 ± 2.32	108 ± 32	292 ± 140	364 ± 508	56 ± 126
4054....	6.48 ± 0.70	108 ± 17	334 ± 64	587 ± 165	46 ± 80
4215....	10.22 ± 0.56	108 ± 6	302 ± 26	420 ± 88	139 ± 18
4220....	12.40 ± 1.39	108 ± 15	308 ± 61	482 ± 173	129 ± 47
4340....	9.47 ± 1.33	108 ± 10	248 ± 40	588 ± 99	65 ± 50
4415....	7.68 ± 1.17	99 ± 16	316 ± 64	798 ± 124	125 ± 44
4454....	4.78 ± 0.90	97 ± 9	233 ± 45	482 ± 112	52 ± 53
4570....	4.36 ± 0.34	97 ± 10	290 ± 49	545 ± 111	58 ± 57
4659...	2.63 ± 1.57	105 ± 3	183 ± 25	206 ± 96	40 ± 17
4769....	3.47 ± 0.62	88 ± 2	38 ± 66	358 ± 31	18 ± 43
4789....	3.65 ± 0.43	104 ± 5	116 ± 66	606 ± 50	0 ± 0
4949....	5.27 ± 0.86	90 ± 15	289 ± 57	551 ± 131	75 ± 43
4958....	4.12 ± 0.47	104 ± 8	220 ± 59	544 ± 88	49 ± 35
5001....	5.62 ± 0.44	92 ± 10	155 ± 62	542 ± 85	37 ± 45
5057....	6.87 ± 0.22	109 ± 11	313 ± 40	633 ± 94	66 ± 32
5169....	7.47 ± 0.44	109 ± 19	330 ± 68	790 ± 136	55 ± 72
5315....	9.61 ± 1.12	108 ± 17	438 ± 50	784 ± 121	101 ± 132
5325....	6.71 ± 0.91	108 ± 11	423 ± 35	789 ± 82	56 ± 161
5329....	8.32 ± 0.34	109 ± 13	403 ± 39	659 ± 115	24 ± 29
5330....	8.48 ± 0.40	125 ± 16	429 ± 64	752 ± 138	50 ± 153
5342....	9.05 ± 0.80	91 ± 20	431 ± 52	779 ± 123	51 ± 56
5373....	6.75 ± 0.58	89 ± 13	280 ± 62	673 ± 111	33 ± 52
5469....	9.15 ± 0.60	100 ± 12	534 ± 28	698 ± 92	32 ± 65
5681....	8.93 ± 0.86	86 ± 7	406 ± 20	665 ± 53	11 ± 106
5692....	8.61 ± 0.56	82 ± 15	501 ± 33	634 ± 100	63 ± 50
5731....	5.17 ± 0.37	86 ± 14	374 ± 43	618 ± 112	21 ± 105
5840....	13.89 ± 0.90	86 ± 10	519 ± 24	516 ± 102	39 ± 44
6195....	3.53 ± 0.22	86 ± 6	248 ± 28	414 ± 71	62 ± 47
6467....	6.79 ± 0.50	92 ± 11	412 ± 19	403 ± 85	23 ± 44
6628....	4.02 ± 0.21	100 ± 6	197 ± 22	290 ± 65	65 ± 26

[a] $F(1350)$ is in units of 10^{-14} ergs s^{-1} cm^{-2} Å^{-1}, and the intensity of the line components is in 10^{-14} ergs s^{-1} cm^{-2}.

e) Reddening

Reddening can greatly affect the relative intensities of the optical and ultraviolet emission lines and the apparent shape of the continuum. The general question of BLR reddening in

TABLE 9

C III] λ1909 COMPONENTS[a]

JD	$F(1350)$	Narrow	Broad	Blue	Si III
4054....	6.482 ± 0.702	17 ± 5	106 ± 10	12 ± 16	13 ± 12
4125....	10.223 ± 0.557	21 ± 8	125 ± 16	16 ± 12	9 ± 24
4220....	12.395 ± 1.389	24 ± 12	150 ± 30	22 ± 16	9 ± 39
4340....	9.469 ± 1.327	18 ± 9	128 ± 15	12 ± 15	11 ± 17
4789....	3.649 ± 0.431	28 ± 4	58 ± 19	10 ± 11	20 ± 14
4958....	4.120 ± 0.465	19 ± 13	95 ± 24	21 ± 14	14 ± 12
5001....	5.619 ± 0.443	13 ± 9	101 ± 12	14 ± 13	19 ± 12
5057....	6.867 ± 0.220	12 ± 4	131 ± 6	22 ± 8	19 ± 11
5169....	7.472 ± 0.436	27 ± 4	130 ± 9	36 ± 11	3 ± 27
5330....	8.477 ± 0.403	26 ± 18	118 ± 26	20 ± 19	9 ± 39
5342....	9.053 ± 0.804	20 ± 13	113 ± 30	15 ± 25	6 ± 46
5373....	6.747 ± 0.585	15 ± 5	113 ± 6	13 ± 6	1 ± 27
5469....	9.146 ± 0.601	19 ± 2	144 ± 6	2 ± 42	0 ± 0
5681....	8.925 ± 0.862	26 ± 9	96 ± 22	25 ± 11	7 ± 34
5731....	5.173 ± 0.373	25 ± 7	102 ± 19	11 ± 22	7 ± 26
5840....	13.889 ± 0.903	17 ± 10	136 ± 30	8 ± 27	13 ± 12
6195....	3.525 ± 0.216	21 ± 3	75 ± 7	9 ± 7	7 ± 9
6467....	6.788 ± 0.499	24 ± 4	112 ± 7	9 ± 9	6 ± 19
6628....	4.016 ± 0.214	24 ± 2	44 ± 14	18 ± 4	9 ± 7

[a] $F(1350)$ is in units of 10^{-14} ergs s^{-1} cm^{-2} Å^{-1}, and the intensity of the line components is in 10^{-14} ergs s^{-1} cm^{-2}.

TABLE 10

Mg II λ2798 COMPONENTS[a]

JD	F(1350)	Narrow	Broad	Blue	Red
3686....	7.137 ± 1.165	14 ± 9	169 ± 21	7 ± 25	15 ± 19
4215....	10.223 ± 0.557	10 ± 3	176 ± 9	5 ± 31	10 ± 6
4220....	12.395 ± 1.389	11 ± 4	133 ± 16	2 ± 36	8 ± 9
4340....	9.469 ± 1.327	19 ± 10	188 ± 33	16 ± 34	8 ± 17
4789....	3.649 ± 0.431	15 ± 8	141 ± 19	10 ± 19	12 ± 15
4958....	4.120 ± 0.465	9 ± 7	138 ± 23	15 ± 22	7 ± 28
5001....	5.619 ± 0.443	8 ± 7	146 ± 20	11 ± 31	11 ± 19
5057....	6.867 ± 0.220	9 ± 9	122 ± 30	20 ± 23	38 ± 17
5330....	8.477 ± 0.403	11 ± 16	152 ± 22	16 ± 26	6 ± 34
5342....	9.053 ± 0.804	9 ± 12	138 ± 36	10 ± 15	19 ± 16
5469....	9.146 ± 0.601	9 ± 6	186 ± 14	12 ± 17	12 ± 32
5681....	8.925 ± 0.862	11 ± 6	225 ± 6	4 ± 37	4 ± 15
5731....	5.173 ± 0.373	9 ± 9	192 ± 19	23 ± 27	12 ± 11
5840....	13.899 ± 0.903	9 ± 9	214 ± 19	13 ± 26	12 ± 24
6195....	3.525 ± 0.216	11 ± 17	149 ± 25	11 ± 15	10 ± 15
6467....	6.788 ± 0.499	6 ± 15	194 ± 23	8 ± 29	7 ± 26
6628....	4.016 ± 0.214	11 ± 9	166 ± 29	13 ± 19	11 ± 24

[a] $F(1350)$ is in units of 10^{-14} ergs s^{-1} cm^{-2} Å^{-1}, and the intensity of the line components is in 10^{-14} ergs s^{-1} cm^{-2}.

AGNs is not completely solved due to theoretical uncertainty in calculating the intensities of the broad hydrogen lines that are the best reddening indicators in gaseous nebulae (e.g., Davidson and Netzer 1979; Netzer and Davidson 1979; Kwan and Krolik 1981; MacAlpine *et al.* 1985). The availability of simultaneous data for NGC 5548, extending from the X-rays to the near-infrared, allows us to compare various reddening indicators. The foreground (galactic) reddening is $E(B-V) = 0.05$ (Burstein and Heiles 1982). The *EXOSAT* observations made in 1984 May indicate a hydrogen column density of 4.1×10^{19} cm^{-2}, corresponding to $E(B-V) = 0.03$ (Branduardi-Raymont 1988). The absence of a 2200 Å feature is consistent with such small reddening, although it is a much less sensitive indicator due to the complex mixture of components in the continuum near this wavelength (see Fig. 3). Thus the X-ray and 2200 Å reddening indicators are consistent with reddening in our Galaxy alone.

Emission-line ratios provide another way of measuring the extinction. As shown by Netzer and Davidson (1979), some weak lines are reliable reddening indicators, but the observational uncertainty in their measurements and the intrinsic variability has made this method almost useless in most AGNs

TABLE 11

BALMER LINES[a]

JD	F(1350)	Narrow	Broad	Red	Blue No. 1	Blue No. 2
			Hα Components			
4054....	6.482 ± 0.702	19.5 ± 0.7	397 ± 2	11 ± 14	25 ± 5	...
4415....	7.677 ± 1.173	...	...	...	...	...
4789....	3.649 ± 0.431	22.4 ± 0.4	276 ± 2	14 ± 7	31 ± 7	2 ± 21
4958....	4.120 ± 0.465	...	...	...	...	...
5001....	5.619 ± 0.443	...	...	...	...	...
5057....	6.867 ± 0.220	16.3 ± 0.8	331 ± 4	16 ± 14	47 ± 9	6 ± 12
5169....	7.472 ± 0.436	...	...	...	...	...
5342....	9.053 ± 0.804	19.4 ± 1.0	444 ± 3	17 ± 16	49 ± 12	9 ± 11
5373....	6.747 ± 0.585	18.3 ± 1.0	388 ± 3	21 ± 12	62 ± 10	9 ± 8
5731....	5.173 ± 0.373	...	...	...	...	...
5840....	13.889 ± 0.903	18.8 ± 0.7	392 ± 2	12 ± 15	29 ± 6	8 ± 6
			Hβ Components			
4054....	6.482 ± 0.702	4.7 ± 0.3	75.4 ± 1.1	7.7 ± 2.6	5.7 ± 2.6	1.0 ± 1.1
4415....	7.677 ± 1.173	6.5 ± 0.6	100.0 ± 2.1	6.8 ± 4.3	13.3 ± 4.3	10.6 ± 3.2
4789....	3.649 ± 0.431	5.0 ± 0.2	49.2 ± 0.6	2.8 ± 3.2	3.6 ± 3.6	2.1 ± 2.2
4958....	4.120 ± 0.465	3.5 ± 0.6	65.3 ± 1.1	3.7 ± 2.1	6.6 ± 2.8	1.3 ± 1.9
5001....	5.619 ± 0.443	5.3 ± 0.3	54.3 ± 0.8	5.4 ± 0.8	7.3 ± 2.7	0.6 ± 2.6
5057....	6.867 ± 0.220	5.0 ± 0.8	62.7 ± 2.2	4.2 ± 4.6	10.9 ± 4.5	2.0 ± 2.1
5169....	7.472 ± 0.436	4.4 ± 2.0	74.3 ± 2.2	7.9 ± 4.4	20.4 ± 4.2	2.9 ± 4.5
5342....	9.053 ± 0.804	3.2 ± 0.6	84.3 ± 1.2	6.9 ± 2.0	8.8 ± 4.1	2.0 ± 3.3
5373....	6.747 ± 0.585	6.0 ± 0.7	94.6 ± 1.6	6.0 ± 3.2	9.3 ± 7.1	2.6 ± 3.8
5731....	5.173 ± 0.373	6.4 ± 0.5	74.2 ± 1.2	4.8 ± 2.4	5.1 ± 3.8	0.7 ± 4.2
5840....	13.889 ± 0.903	7.1 ± 1.3	83.1 ± 2.7	9.8 ± 4.5	10.9 ± 4.1	1.7 ± 4.7
			Hγ Components			
4054....	6.482 ± 0.702	1.7 ± 0.2	29.9 ± 0.5	4.3 ± 0.9	2.9 ± 2.2	0.5 ± 0.5
4415....	7.677 ± 1.173	1.7 ± 0.4	52.4 ± 1.1	3.9 ± 4.9	10.1 ± 2.5	1.3 ± 1.1
4789....	3.649 ± 0.431	2.6 ± 0.3	15.4 ± 1.6	4.4 ± 0.8	1.9 ± 1.4	0.6 ± 1.1
4958....	4.120 ± 0.465	2.2 ± 0.5	23.5 ± 1.4	4.9 ± 1.4	1.5 ± 2.4	0.6 ± 1.5
5001....	5.619 ± 0.443	1.4 ± 0.2	22.0 ± 0.4	2.6 ± 0.7	1.5 ± 1.9	0.6 ± 0.4
5057....	6.867 ± 0.220	2.0 ± 0.1	32.3 ± 0.2	0.7 ± 2.2	2.2 ± 0.6	0.8 ± 0.7
5169....	7.472 ± 0.436	1.0 ± 0.8	40.4 ± 0.8	3.2 ± 3.2	7.2 ± 1.8	3.2 ± 0.8
5342....	9.053 ± 0.804	...	...	...	...	...
5373....	6.747 ± 0.585	2.7 ± 0.7	33.1 ± 1.0	5.4 ± 1.8	9.2 ± 2.9	2.8 ± 3.4
5731....	5.173 ± 0.373	4.9 ± 0.2	31.9 ± 0.7	1.4 ± 3.3	3.5 ± 1.9	2.0 ± 0.6
5840....	13.889 ± 0.903	5.0 ± 0.2	49.6 ± 0.5	1.2 ± 3.5	4.5 ± 1.4	2.6 ± 1.5

[a] $F(1350)$ is in units of 10^{-14} ergs s^{-1} cm^{-2} Å^{-1}, and the intensity of the line components is in 10^{-14} ergs s^{-1} cm^{-2}.

TABLE 12

He II λ1640 COMPONENTS[a]

JD	F(1350)	Narrow	Very Broad	[O III]1663	λ1580
3686....	7.137 ± 1.165	15 ± 11	109 ± 72	33 ± 18	76 ± 25
4054....	6.482 ± 0.702	18 ± 7	74 ± 81	19 ± 10	45 ± 31
4215....	10.223 ± 0.557	15 ± 8	96 ± 62	11 ± 12	85 ± 21
4220....	12.395 ± 1.389	17 ± 29	96 ± 250	18 ± 28	56 ± 84
4340....	9.469 ± 1.327	15 ± 29	133 ± 148	56 ± 22	118 ± 53
4415....	7.677 ± 1.173	23 ± 30	203 ± 162	37 ± 53	82 ± 36
4454....	4.781 ± 0.901	18 ± 10	70 ± 124	41 ± 12	81 ± 20
4570....	4.357 ± 0.338	14 ± 11	85 ± 85	20 ± 22	100 ± 14
4659....	2.626 ± 1.566	18 ± 5	28 ± 145	27 ± 9	31 ± 25
4769....	3.469 ± 0.620	15 ± 11	71 ± 108	6 ± 27	41 ± 37
4789....	3.649 ± 0.431	15 ± 10	96 ± 72	14 ± 11	85 ± 24
4948....	5.267 ± 0.856	20 ± 15	91 ± 155	21 ± 14	53 ± 52
4958....	4.120 ± 0.465	15 ± 12	92 ± 93	15 ± 12	51 ± 27
5001....	5.619 ± 0.443	14 ± 11	92 ± 82	14 ± 11	15 ± 25
5057....	6.867 ± 0.220	23 ± 9	130 ± 78	17 ± 12	69 ± 33
5169....	7.472 ± 0.436	14 ± 10	83 ± 81	14 ± 10	80 ± 17
5315....	9.613 ± 1.119	24 ± 25	164 ± 173	11 ± 55	52 ± 108
5325....	6.710 ± 0.910	36 ± 12	136 ± 145	11 ± 38	46 ± 85
5329....	8.321 ± 0.336	23 ± 8	72 ± 127	28 ± 19	43 ± 41
5330....	8.477 ± 0.403	21 ± 9	121 ± 73	47 ± 10	93 ± 19
5342....	9.053 ± 0.804	22 ± 19	152 ± 125	13 ± 30	80 ± 54
5373....	6.747 ± 0.585	21 ± 12	82 ± 152	12 ± 23	60 ± 47
5469....	9.146 ± 0.601	19 ± 21	191 ± 98	9 ± 42	18 ± 40
5681....	8.925 ± 0.862	23 ± 20	147 ± 150	16 ± 29	79 ± 55
5731....	5.173 ± 0.373	18 ± 10	117 ± 72	5 ± 36	48 ± 19
5840....	13.889 ± 0.903	17 ± 21	140 ± 122	20 ± 18	47 ± 38
6195....	3.525 ± 0.216	16 ± 6	87 ± 52	33 ± 16	46 ± 23
6467....	6.788 ± 0.499	20 ± 7	87 ± 81	16 ± 9	41 ± 40
6628....	4.016 ± 0.214	14 ± 4	62 ± 42	22 ± 11	75 ± 8

[a] $F(1350)$ is in units of 10^{-14} ergs s^{-1} cm^{-2} Å^{-1}, and the intensity of the line components is in 10^{-14} ergs s^{-1} cm^{-2}.

observed so far. The He II λ1640/λ4686 line ratio is one of the best ratios (Netzer and Davidson 1979; MacAlpine *et al.* 1985; Netzer, Elitzur, and Ferland 1985). Netzer *et al.* (1985) calculated the He II spectrum under a variety of conditions, including all processes such as Lyα pumping and optical depth in the He II lines. They found that the theoretical He II λ1640/λ4686 line ratio in "typical" broad-line region (BLR) clouds is about 9–11. The same ratio in the narrow-line region (NLR) is much smaller, 4–6, depending on the electron density. The He II lines in NGC 5548 do not show any sign of the ordinary broad component (FWHM = 5000 km s^{-1}), and we could only measure the intensities of the narrow and the very broad (FWHM = 10,000 km s^{-1}) ones. The narrow-line component ratio is 11.2 ± 4.1, and the very broad line component ratio is 6.9 ± 3.4 (see also § Vc). The ratio of the narrow components presents a real problem, since it is inconsistent with the theoretical prediction for all $N_e \leq 10^8$ cm^{-3}. From the results presented below in § IVc(i), a higher than normally assumed density is also suggested by other narrow lines. Possible alternatives could be overestimation of the galactic reddening toward NGC 5548 [adopting $E(B-V) = 0.03$, instead of the 0.05 we have assumed, decreases the ratio by about 15%] or a 10% systematic calibration of the absolute flux level of *IUE*. Another possibility is that the line ratio could be affected somewhat by the different spectral resolution between the optical and ultraviolet data. However, we note that the He II line ratio observed in the bright Seyfert 2 galaxy NGC 3393 (Diaz, Prieto, and Wamsteker 1988), where no broad lines are observed, is 9 ± 2, also larger than predicted for a low-density gas.

The measured ratio for the very broad components, combined with the calculations by Netzer *et al.* (1985), could suggest that there may be some intrinsic reddening in NGC 5548 corresponding to $E(B-V) = 0.12 \pm 0.10$. This reddening, if it exists, affects the region where the very broad emission-line component originates, but not necessarily the other components. We have no way of knowing whether it affects the nonstellar continuum. Note here that the complex variations observed in the He II lines (§ V) could mean that they are affected by the physical conditions much more than originally suspected, in which case no evidence for instrinsic absorption can be concluded.

IV. RESULTS

The numerical data on which the following discussion is based are: continuum measurements in Table 4, line profiles in Table 6, narrow-line intensities in Table 3, broad-line components in Tables 7–12, and integrated line intensities in Table 5. We have not made any corrections for possible internal reddening, and all our quoted results include the correction for galactic extinction only, $E(B-V) = 0.05$.

a) *Continuum Variability*

Continuum variations in AGNs supply information on the source size and the shape of the ionizing continuum. In addition, the relations between the line and continuum variability allow us to test photoionization and other excitation mechanisms proposed for the BLR.

The UV and optical (FES) continuum light curves of NGC 5548 are shown in Figure 6 together with the B component of C IV λ1549 and Mg II λ2798. The dominant variability during the time covered by the observations, which were made with an average sampling interval of 98 days, is the large decrease and recovery in flux between JD 2,444,200 (1979 December) and JD 2,445,300 (1982 November)—about 1000 days. The twofold time of this variation is about 270 days. Some data, e.g., between 1984 February and May, indicate that rather large changes can also occur on shorter time scales, in this case an increase by a factor of nearly 3 over 100 days. Correlation studies of the light curves in different continuum windows show that the variations at all wavelengths are well correlated with the variation at 1350 Å (Rodriguez-Pascual, Santos-Lleo, and Clavel 1989). This is also true for the FES light curve, and there is no evidence for short-term variations (<4 days) with similar amplitudes. The data taken within a single *IUE* observing shift do not indicate variations greater than 3% on time scales of the order of 6 hr (see the Appendix). Therefore, we conclude that the dominant variability time scale of the continuum variations of NGC 5548 sampled by our data is of the order of 1 yr. The suggested existence of variations with shorter time scales is confirmed by the more regular observations made every 20 days during 7 months in 1988 which indicate persistent variation on the order of 50 days (Rodriguez and Wamsteker, private communication).

The flux densities in the line-free windows at 1350 Å (width of 40 Å) and 5500 Å (width of 100 Å) have been used to determine the spectral index α, and its variations (Fig. 7). We find:

$$\alpha(1350/5500) = (0.7 \pm 0.2) - (0.04 \pm 0.02) \times F(1350) \times 10^{-14} \text{ ergs s}^{-1} \text{ cm}^{-2} \text{ Å}^{-1}, \quad (1)$$

significant at the 98% level. Thus the spectrum hardens slightly with increasing UV continuum luminosity. This is contrary to the trend seen in X-rays—the *EXOSAT* ME (2–6 keV) hard-

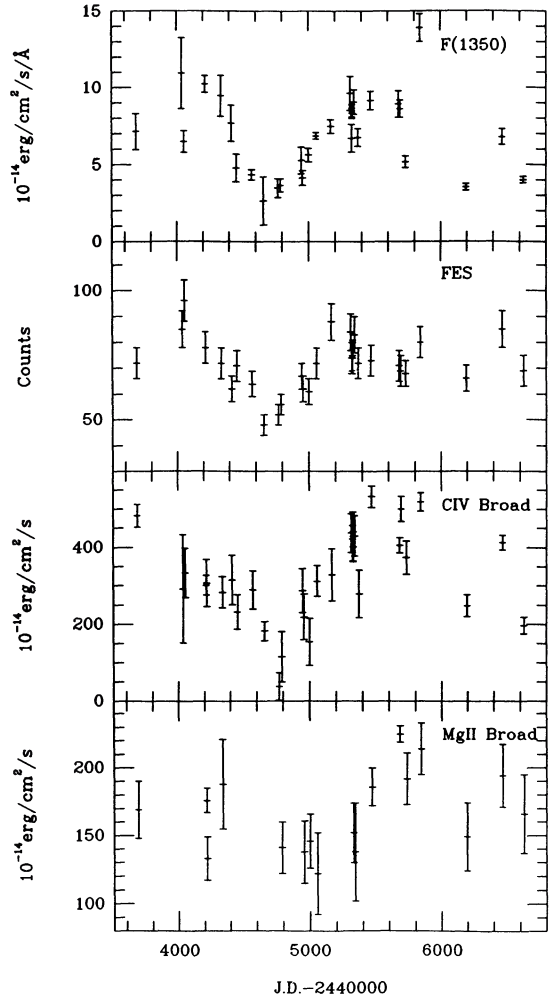

FIG. 6.—Light curves of NGC 5548. From top to bottom: The UV continuum $F(1350)$; the *IUE*–FES corresponding (5500 Å); the B component (FWHM = 5080 ± 200 km s^{-1}) of C IV λ1549; the B component (FWHM = 5250 ± 100 km s^{-1}) of Mg II λ2798. All light curves show the large decrease in the period of 1981–1982. The decrease in amplitude between 1350 and 5500 Å can be accounted for by the starlight contribution inside the aperture (see text), and the two light curves appear identical. The decrease and increase for both C IV λ1549 and Mg II λ2798 seem slightly delayed with respect to the continuum. Due to the sampling in the data, it is not possible to determine with certainty the length of the delay, but cross-correlation suggests that the Mg II λ2798 delay is about twice that of C IV λ1549. Note also the differences in amplitude of the light curves ΔM(Mg II) = 0.6 mag, $\Delta M[F(1450)]$ = 1.8 mag, and ΔM(C IV) = 2.5 mag.

ness ratio decreases with increasing ME brightness (Branduardi-Raymont 1988). This supports the idea that the hard X-rays are independent of the radiation seen in the UV. Such behavior of the UV continuum slope would indicate that the soft X-ray excess seen in NGC 5548 (Pounds and Turner 1988) represents the high-frequency end of the UV-optical power-law spectrum. Such extension of the UV spectrum in AGNs to shorter wavelengths is also suggested by the results from Reimers *et al.* (1989) in the high-redshift AGN HS 1700+6416.

b) Fe II *and Balmer Continuum Variability*

No significant variation is found for any of the Fe II blends from 3000–7000 Å, so these Fe II multiplet strengths do not seem to be correlated with the strength of the ionizing continuum. On the other hand, some systematic variation for the Fe II(UV) is clearly indicated (see Fig. 8 and also Figs. 3*a* and 3*d*). The variation in Fe II(UV) appears closely related with the variation in Mg II λ2798, which is significantly delayed with respect to the continuum variations (see Fig. 6).

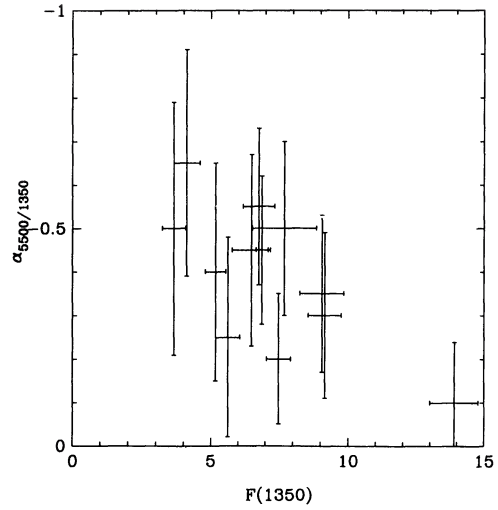

FIG. 7.—The power-law index $\alpha(\lambda 5500/\lambda 1350)$ of the variable AGN continuum as a function of its brightness $F(1350)$. This behavior is contrary to that seen in the X-rays, where the continuum index becomes softer when the (2–10 KeV) brightness increases.

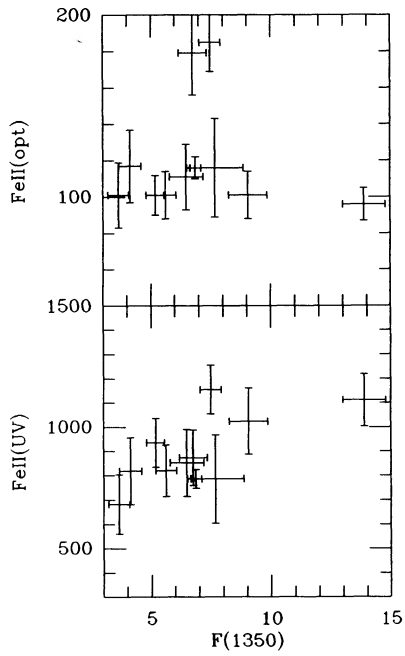

FIG. 8.—The intensity of Fe II multiplets as a function of continuum intensity $F(1350)$. This was measured using the models of WNW (see § IIIc) in the optical from 3504 to 6882 Å (*top*) and in the UV from 1456 to 2998 Å (*bottom*). The two high points in the optical are associated with the epochs 1982 June (only a red optical spectrum was available) and 1983 February (LW *IUE* spectra very noisy), which are considerably less certain than the other points. See also Fig. 1 and Table 5. Contrary to the Fe II UV, the Fe II opt does not show a systematic variation with the continuum brightness. The variation in Fe III UV appears somewhat delayed with respect to the continuum variations, similar to Mg II λ2798. The errors are as for the continuum determination.

The Balmer continuum intensity is very closely correlated with the UV continuum. The resulting relation is:

$$I(\mathrm{Bac}) = (207 \pm 22) \times F(1350) - (103 \pm 152) \times 10^{-14} \text{ ergs s}^{-1} \text{ cm}^{-2} . \quad (2)$$

In deriving this relation, we have excluded the data for 1984 May, which deviate strongly, in this and some other relations, from the general trend set by all other epochs (see also Fig. 9). There is also a tight correlation between the Lyα intensity and the Balmer continuum strength:

$$I(\mathrm{Bac}) = (1.52 \pm 0.12) \times I(\mathrm{Ly}\alpha) - (79 \pm 104) \times 10^{-14} \text{ ergs s}^{-1} \text{ cm}^{-2} , \quad (3)$$

significant at the 99.9% confidence level. This relation (3) and equation (1) for the continuum slope allow us to analyze the large UV data set in a way that is identical to that used for the epochs with simultaneous UV and optical data. Although it would appear more obvious to use relation (2) between Balmer continuum and the $F(1350)$ flux, the results for 1984 May invalidate the general applicability of this relation, and we prefer the use of equation (3). After subtraction of the power-law and Balmer continuum, the Fe II can also be fitted.

c) Emission Lines

Table 5, giving the total line intensities, is included for comparison with previous studies of line variability in AGNs, where, in general, no decomposition into line components was attempted. Only epochs with full UV and optical coverage are listed. The integrated line ratios in NGC 5548, at all brightness levels, are quite similar to those indicated in Table 5 for NGC 4151.

The aim of this project was to measure the individual line components and to use them to derive information that cannot be obtained from the integrated line intensity. Below we discuss line ratios and line-continuum correlations derived for the different emission-line components in NGC 5548 and use them to interpret the physical conditions in a way not yet attempted for other Seyfert galaxies.

i) Narrow Lines

Our definition of "the narrow-line component" is related to the resolution of our data: the FWHM is about 1400 km s^{-1} in the UV and generally about 700 km s^{-1} in the optical. The narrow-line measurements in Tables 3 and 7–11 represent the intensities of Gaussian profiles with a width as given in Table 6. The uncertainties associated with each component, as listed in the tables, are derived from the fit, as explained in the Appendix. For the weaker components, some additional uncertainty in the intensities may have been introduced by the fitting procedure itself. For the strongest UV lines, the narrow component contributes 10%–15% of the total line flux, while for the Balmer lines this amounts to only 5%. Quite small variations in the broader components can have an unexpectedly large influence on the measurement of the narrow-line flux. We suspect that this is the case for Hβ and possibly Hγ, where the scatter in the results is larger than would be expected on the basis of the error estimates. For most of the narrow lines, except Lyα, no systematic variability could be established, and therefore the excess scatter seen in some narrow lines is most likely due to the actual fitting procedure.

A comparison of the narrow-line intensities with those found in one of the few Seyfert 2 galaxies for which similar data exist, NGC 3393 (Diaz, Prieto, and Wamsteker 1988), is included in Table 3. A few differences are worth noting. The extreme strength of the C IV λ1549 line, more than 4 times as strong relative to Hβ in NGC 5548 compared with NGC 3393, is obvious. Whether this indicates a real difference in the conditions in the corresponding regions of the Seyfert 1 and the Seyfert 2 can only be established from the data with higher resolution, sufficient to assure that we explore the same velocity domain in the two galaxies. However, for the optical forbidden lines, which show less dramatic differences and for which no resolution problems exist, a comparison of the lines in NGC 5548 and NGC 3393 suggests that the electron density in the NLR of the Seyfert 1 is considerably larger. This is indicated by the relative strength of the Hβ, [O III] λ5007, [O III] λ4363, and [Fe VII] λ6087 lines. We suggest that, in NGC 5548, regions with relatively high density ($N_e \geq 10^5$ cm^{-3}) dominate the narrow-line emission, while for NGC 3393, the density in the narrow-line region is considerably lower. The difficulties presented by the narrow-line ratios of He II in the two galaxies have been discussed in the context of the reddening estimates (§ III*e*) and could be related to the high density. Also, the strength of O III] λ1663 suggests a con-

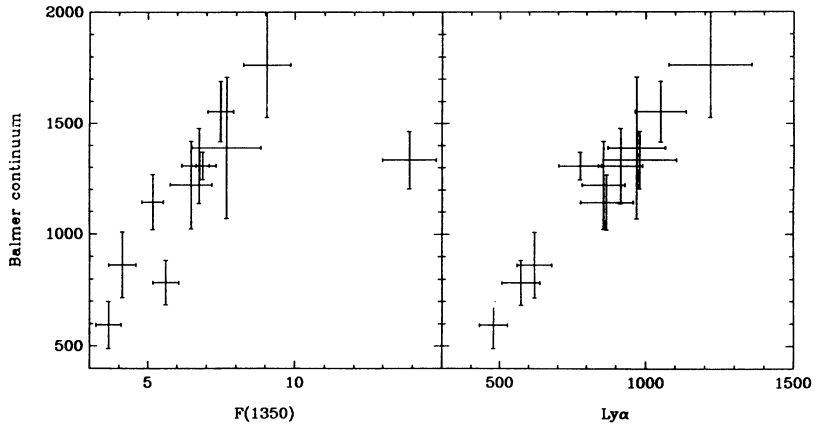

FIG. 9.—The variations in the Balmer continuum (Table 5) are shown here as a function of the continuum intensity $F(1350)$ (*left*) and as a function of the total intensity of the Lyα λ1216 emission line (*right*). These data correspond to the relations (2) and (3). Since the relation with Lyα is much tighter and does not show any deviating points, we used this to correct those dates, when only UV data were available, for the contribution of the Balmer continuum. The errors are as for the continuum determination.

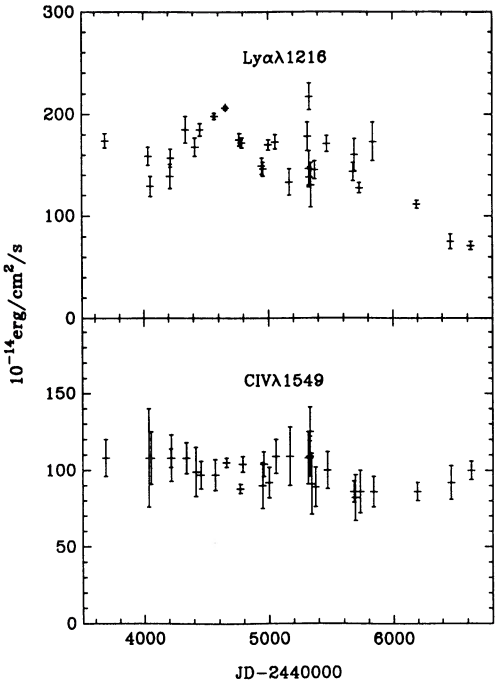

FIG. 10.—Light curves for the narrow lines of Lyα and C IV λ1549. The variability of Lyα contrasts sharply with the stability of C IV. It is suggested that the variation in Lyα is a delayed response of the NLR to the large continuum variation in 1981. This would suggest a size for the NLR in NGC 5548 of some 3 lt-yr, comparable to the results found for 3C 390.3 by Clavel and Wamsteker (1987). The nonvariability of C IV is not easy to explain.

siderably higher density, possibly as high as 10^7 cm^{-3} for the NLR in NGC 5548. An alternative explanation of the strength of O III] λ1663 could be a high T_e of some 35,000 K, which is not supported by other temperature-sensitive line ratios.

The only exception to the constancy of the narrow lines is Lyα, which shows significant variations over the time of observation (Fig. 10). Unfortunately we do not have optical data for the interval when Lyα showed this strong drop. Although the variations in the narrow component are quite pronounced, they do not appear to be correlated with the continuum variations. More recent data show that the narrow Lyα is back up to its intensity level of 1981, and one possibility is that the drop in the narrow component is a delayed reaction to the large continuum decrease of middle 1981. If this is the case, then we may be seeing a similar behavior as in 3C 390.3 (Clavel and Wamsteker 1987), suggesting a size of the NLR of ~3 lt-yr. The lack of variability in C IV λ1549 is difficult to understand, but in the absence of contemporaneous Balmer line observations, it is difficult to draw any firm conclusion.

ii) *The Broad Emission Lines*

The methods of decomposing the observed line profiles do not assure the physical reality of the Gaussian components. However, the results obtained strongly suggest that the standard components identified (Table 6) represent gas which behaves under identifiably different physical conditions. We describe their variation and correlation with the continuum properties, and in § V we discuss implications for the theory of AGNs.

The VB component is present in Lyα, C IV λ1549, He II λ1640, He II λ4686, and He I λ5876. The B component is present in nearly all permitted lines of both high and low excitation, with the notable exception of the helium lines. The red and blue components are present in most low-ionization lines, while the blue component is also present in C IV λ1549. The narrow component is present in all lines. The width of the red and blue line components is clearly larger than that of the narrow lines, but distinctly narrower than the B component.

The data in Table 6 show that the central velocity of the B line is indistinguishable from that of the narrow lines, so the gas emitting at these velocities has no systematic radial motion. This is in contrast to the VB line, which is systematically blueshifted by about 2000 km s^{-1}. There exist clear indications, from the analysis of absorption lines, that there is outflow motion in the AGNs NGC 4151 (Bromage *et al.* 1985) and NGC 3783 (Wamsteker and Barr 1985). However, our observations are the first to indicate that the assymetry may be present in one broad-line component and not in others. This has interesting implications for the geometry and dynamics of the BLR in NGC 5548.

The results listed in Tables 7–12 show that all broad-line components are variable and that the relations with the continuum are not always simple. We discuss these variations by comparing them to the normalized $F(1350)$, where the normalization is relative to the lowest observed value (Figs. 11 and 13). For the optical-UV data, this is 1981 July (JD 2,444,790) and for the UV only, this is the averaged data of 1981 February, June, and July (JD 2,444,659, 4770, 4790). Individual light curves are shown only in special cases such as the variations of the B component of C IV λ1549 and Mg II λ2798 in Figure 6, the VB components of C IV λ1549 and He II λ1640 in Figure 12, and the narrow Lyα and C IV λ1549 in Figure 10.

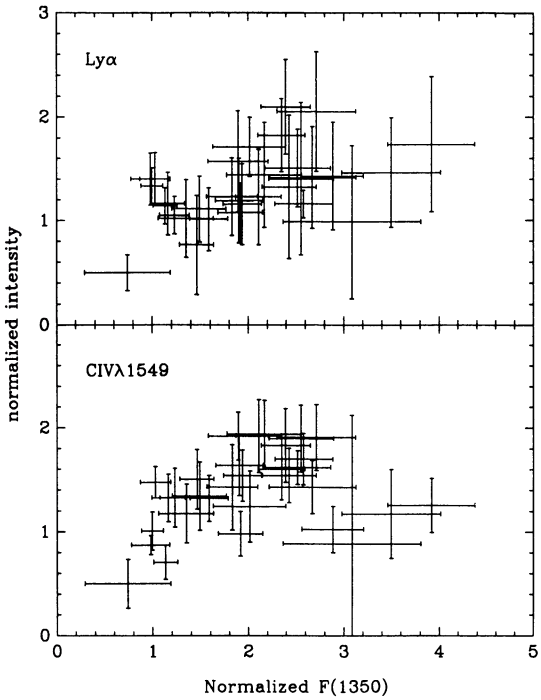

FIG. 11.—This figure shows the relative variations of the VB component with $F(1350)$ UV continuum intensity. For both lines shown—Lyα and C IV λ1549—a significant correlation is indicated. Note the turnover in the C IV line strength (see also Fig. 5). If this represents the onset of ionization of C^{3+} into C^{4+}, it would suggest matter boundedness for the region emitting the VB line component. On the other hand, this could also suggest asymmetrically sampled hysteresis behavior.

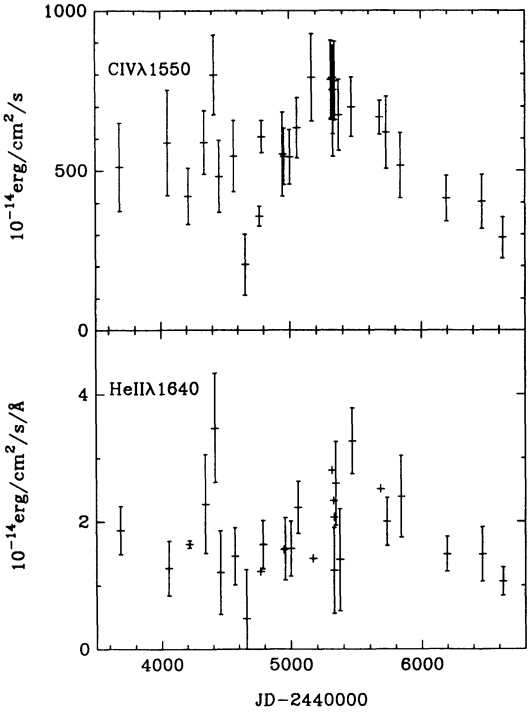

FIG. 12.—Light curves of the VB components of C IV λ1549 and He II λ1640. The variability of these lines is quite well correlated with the UV continuum (Fig. 6, top). Note the rather monotonic decrease after day 24,455,000, which shows no evidence of the erratic variations seen in the continuum light curve. Since the formal errors (see Appendix) on He II are rather large, we show here the error bars on the peak intensity, which is better defined for this weak VB component, since no B component is present in the lines of He II.

The VB component.—The VB line intensities as a function of $F(1350)$ are shown in Figure 11. The Lyα intensity is proportional to the continuum strength at half the amplitude, while similar behavior is seen for C IV λ1549 with an amplitude roughly equal to that of the continuum. Also, the C IV λ1549 line reaches its maximum intensity at $F(1350) = 8 \times 10^{-14}$ ergs s^{-1} cm^{-2} Å^{-1}, considerably below the peak continuum observed. Above this intensity, the strength of the VB C IV λ1549 line decreases with increasing continuum. To illustrate the increase and subsequent decrease of this line component, we show in Figure 5 the decomposition of C IV λ1549 into its component at four epochs.

Since the VB He II λ16400 is weak and does not show the B component, we choose to show the peak intensity of the line (which has a smaller error than the intensity) in Figure 12 together with the intensity of the VB component of the C IV λ1549 line. The VB component of He II λ1640 follows the continuum variations quite closely (Fig. 6), and its light curve is similar to that of the VB component of C IV λ1549. He II λ1640 and the corresponding He II λ4686 optical line are very interesting, since neither show any B component (Fig. 4), and both are highly variable. Further discussion and comparison with theory for these lines is given in § V.

The B component.—The variability of the B component of the lines as a function of continuum brightness is shown in Figure 13. There is no question about the response of these line components to variations in $F(1350)$. The changes of the Balmer lines are such that the Balmer decrement becomes smaller with increasing continuum luminosity. Variations of this nature have been reported by de Bruyn (1980) for the Seyfert 1 galaxy NGC 7469. Our observations confirm this behavior in another AGN and show that it is due to the B component only. Such a trend must be related to the Balmer optical depth (§ V). The Mg II λ2798 line, which is also clearly variable, although with a relatively small amplitude, shows essentially a scatter diagram in a diagram like Figure 13. This is caused by the fact that there is a strong indication that Mg II λ2798 line responds to the continuum variations with a considerable delay (see Fig. 6). Cross-correlation between this line and the continuum indicates a peak at 100 ± 90 days. Since the UV data are somewhat closer sampled in the strong rise in late 1981 than in the decrease, the significantly larger delay then shown by the Lyα and C IV λ1549 causes the relation with $F(1350)$ to appear like a scatter diagram.

The relative intensity of the C IV λ1549 and the C III λ1909 B components, during different activity phases, has been measured and found to be almost constant as a function of time and $F(1350)$. This line ratio is thus very insensitive to the value of the ionization parameter. The Lyα/C IV λ1549 ratio for the

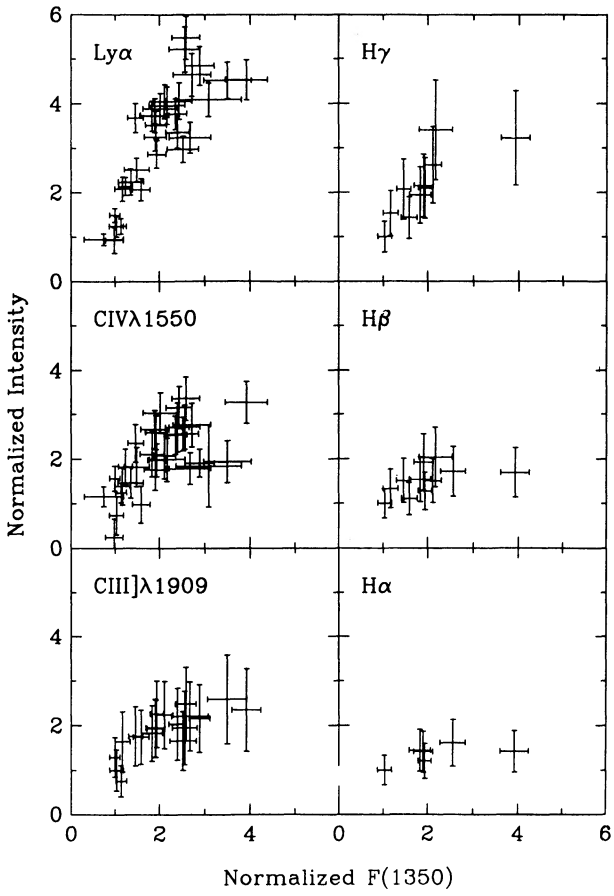

FIG. 13.—Relative variations in the intensities of some of the B line components [FWHM = 5000 km s^{-1} with the UV continuum $F(1350)$]. All data are shown relative to the faintest value observed in our data (see § V*a*). There is no dount that $F(1350)$ is indeed a measure of the ionizing continuum and the strong correlations shown for all lines are giving strong support for the photoionization models for AGNs. The decrease of the Balmer decrement with increasing $F(1250)$ is easily seen. The points at $F(1350) = 4$ are for the observations of 1984 May, which correspond to the fastest large-amplitude variation in our data, and its behavior is somewhat distinct from the trends shown by all other data.

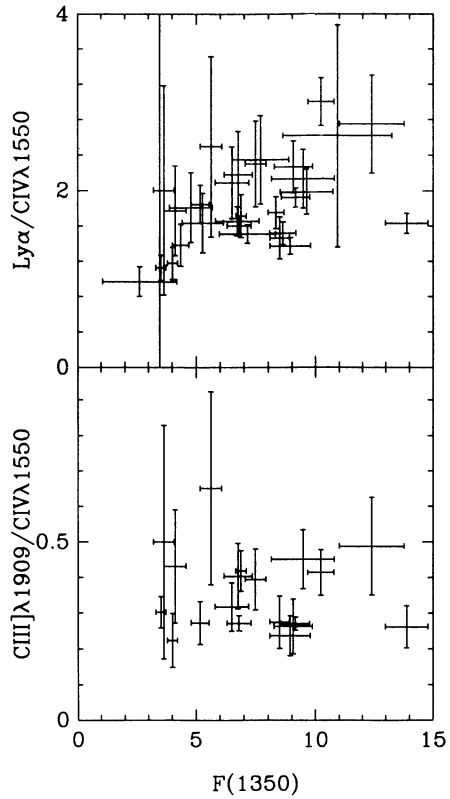

FIG. 14.—Flux ratios Lyα/C IV λ1549 and C III] λ1909/C IV λ1549 for the B component in those lines. The combined constantness of this last one, together with the variations of the first, suggest that this region represents a physical entity in itself. The constant value of the carbon line ratio suggest a high ionization parameter ($U > 0.1$) and thus indicates that the C III]/C IV ratio is not a very good excitation indicator, as was previously thought. The Lyα/C IV λ1549 ratio for the B component is similar to that of the VB component when the continuum is faint. The increase with increasing continuum can be reproduced with a relatively low energy cutoff for the UV-optical power law at about 60 eV.

B component is clearly increasing with $F(1350)$ (Fig. 14). When the continuum is faint, the ratio is very close to that of the VB component (0.9 ± 0.3), whereas, when the continuum is bright, it is similar or even slightly higher than the value found for the NLR of Lyα/C IV λ1549 = 1.8 (Table 3). Thus, an increasing ionizing flux corresponds to a decrease in the relative intensity of a high ionization line such as C IV λ1549. This behavior is not unique to NGC 5548 and has been observed in other AGNs (see, e.g., Wamsteker and Colina 1986).

The blue and red components.—Although these carry only a small fraction of the total line flux, comparable to the narrow lines, they represent independent entities in the broad-line profile which cannot be accounted for by any other means. Their presence is illustrated in Figure 6 for the Hβ line and for the C IV λ1549 line. In most cases, it is difficult to establish the details of their variability, since they have large formal errors and the measured line intensity is quite sensitive to small details of the final line fits of the major components of the lines. However, a few characteristics can be firmly stated. For Hβ, both the blue and the red components are varying coherently, i.e., the linear relation between the two components passes through zero, while the amplitude of the blue component is approximately 1.5 times that of the red component. Both components are directly proportional to the continuum brightness $F(1350)$. The measurement uncertainties are too large for Mg II λ2798 to determine the nature of the variability, but both components are clearly present in this line and are variable. In C IV λ1549, the blue component is the only one present, and a relation with the continuum is indicated but cannot be firmly established, as is also the case for the blue component of C III] λ1909. The presence or absence of the red component in C III] λ1909 could not be determined due to its location at the edge of the *IUE* short-wavelength camera. Note that the existence of a blue component in Lyα could not be determined due to the merging of the geo-coronal line at the short-wavelength side. The red component is definitely absent equally to the C IV line. The width of these lines and their strong variability suggests that they are associated with the BLR rather than with the NLR. The detailed line analysis of the Hβ line in Fairall 9 (Wamsteker *et al.* 1985) showed the presence of a similar red component in this object, suggesting that such components could be quite common and do significantly affect the overall line shape of the broad lines.

V. DISCUSSION

Our observations of NGC 5548 are unique since they are the first to show all the important UV and optical emission lines during different phases of activity, with a signal-to-noise large enough to separate the lines into components. We could, therefore, analyze light curves for individual components and discuss line ratios for each. It is evident from the data that some lines are very different from others, and statements referring to "total line intensity ratio" may not be very meaningful. Below we discuss some of the more important findings of our work and emphasize new aspects related to our unique set of data.

a) Hydrogen Lines

There have been many theoretical investigations of the hydrogen spectrum in AGNs showing that the relative intensity of the lines is a complicated function of the density, temperature, and optical depth (Davidson and Netzer 1979; Kwan and Krolik 1981; Elitzur 1984; Puetter and Hubbard 1987; Collin-Souffrin *et al.* 1986). Notable problems are the Lyman/Balmer line ratio and the Balmer decrement. In NGC 5548, the total Lyα/Hβ ratio varies between about 14 and 22, but the ratio of the B component varies between 5 and 12. This ratio for the VB components is very large, since this component is nonexistent in Hβ. The combination of these two rather distinct line components gives rise to the anomalously high line ratio. When seen separately, the results are more in line with the general results of photoionization theory. The narrow lines are consistent with what would be expected from normal case B recombination theory.

Our observations (Fig. 13) show that the B component of the lines respond differently to the continuum changes. Lyα responds with the largest amplitude, then Hγ, Hβ, while Hα hardly varies at all. An increase of ionizing flux must be followed by an increased Balmer optical depth, since the ionization front extends deeper into the gas in a radiation-bounded situation. The observations show that this inevitable increase in τ(Balmer) results in a decrease of the Balmer decrement, in agreement with the prediction of some calculations. Older and less extensive observations by de Bruyn (1980) of the Balmer line ratios in NGC 7469 show a similar behavior. The Balmer decrement observed in each of the different phases of activity in NGC 5548 can be compared to a *single* observation in another

AGN. Thus, ionizing flux variation by itself can explain most of the observed range of Balmer decrements in AGNs, and there is no need to invoke changes in density. While the theory of the hydrogen lines in AGNs is not yet fully developed, we believe that the information supplied here could help resolve questions like what is the "typical" optical depth in Hα and what densities are required to produce the observed line ratio. Finally, the observed large variation in the Balmer continuum seems to follow Lyα more than any other line. This, plus the fact that we observe the largest contribution to the weakly variable Hα from the B component, indicates that much of the flux in the Balmer continuum could originate in the VB gas.

b) Carbon Lines

Discussion of the carbon lines must be separated into two parts: the B and the VB components.

The B line component is present in both C^{3+} and C^{2+} lines. Figure 14 shows that the C III] λ1909/C IV λ1549 line ratio changes very little as a function of $F(1350)$ for the B component. Thus, we must find values of the ionization parameter U, for which this line ratio is least sensitive to variations in U. Recent theoretical work (Ferland and Persson 1989; Netzer 1987, 1989) indicates that this is the case for those values of U (0.1–1.0) needed to explain the small dimension of the BLR in NGC 5548 of <14 lt-day suggested by Netzer *et al.* (1989). These very small changes in this line ratio are therefore not consistent with the previously assumed values for U (0.01) used in theoretical studies of AGNs.

The observed increase in Lyα/C IV λ1549 ratio for the B component (Fig. 12) cannot easily be reproduced by the classical photoionization model calculations. More recent calculations (e.g., by Ferland 1987) show that such behavior can be reproduced if the cutoff of the UV-optical power law occurs at lower energies (60 eV or 200 Å) than was previously thought to be the case. Such a cutoff is still consistent with the short-wavelength extension found for the high-redshift QSO HS 1700+6416 (Reimers *et al.* 1989). These results are similar to those, giving rise to the general problem for this line ratio in high-luminosity objects as discussed by Netzer (1989).

The behavior of the VB C IV λ1549 and its relation to the VB Lyα is very interesting. The component has a blue asymmetry, of about 2000 km s^{-1}, and the ratio increases with $F(1350)$ only to a certain point beyond which Lyα continues to increase with $F(1350)$ but C IV λ1549 seems to saturate (Fig. 11). The line asymmetry could indicate something about the geometry in the innermost part of the BLR. For example, a combination of outflow motion with obscuration (by, e.g., a central accretion disk) could give the observed assymetry of the VB component. The B component is further away in this case and is not obscured (by the small central disk). In this picture, the velocity decreases outward, which may indicate large acceleration in the inner parts and slowing down further out. This is also consistent with the indications that the gas associated with the VB component has higher excitation conditions compared with the B gas component. Obscuration by dust is less likely in this case, since the obscuring material can only be present very close to the center. On the other hand, real differences in the physical conditions of the gas which emits similar line components could give rise to such behavior as seen here, e.g., in the B component for C IV λ1549 and the B component of Mg II λ2798. Although observationally these have the same kinematic signature, the large differences in the cross-correlations with the continuum, suggesting delays of less than 50 days and nearly 100 days, respectively (see also Fig. 6), indicate that even the line ratios of the same components might not give direct information on the instantaneous state of the broad-line gas. The results indicate that some past variability behavior could actually be needed to interpret the line ratios in AGNs. Since our data are not sampled frequently enough with respect to the indicated delays, it is not possible to discriminate the possible explanations of the decrease of the VB component of C IV λ1549 at large values of $F(1350)$, such as:

1. Matter-bounded conditions and ionization from C^{3+} to C^{4+}.
2. Different response characteristics of Lyα and C IV λ1549 to the continuum variations (e.g., noncoincidence of hysteresis loops in the F[continuum] vs. line flux diagrams).
3. Dramatic variations in the ionization parameter U, even though this appears in contradiction with further results obtained here.

Observation of the behavior of higher excitation lines such as O VI λ1034, which is not accessible in low-redshift objects such as NGC 5548 with the presently available instrumentation, could help in clarifying this.

c) Helium Lines

The helium line spectrum of NGC 5548 is most interesting because of the large observed variations and because those line profiles only a show the VB component (Figs. 3, 4, and 12).

The variations of the He II λ4686 line in this galaxy have been subject of two papers (Peterson and Ferland 1986; Kallman and Elitzur 1988). Peterson and Ferland noted a large flux increase of the line, in 1984 March, which was not followed by a comparable increase in Hβ. They interpreted this as an "accretion event" near the center, i.e., a supply of new material at the location where the excitation is high enough to preferably produce He^{++}. Kallman and Elitzur argued that the observations may be explained within the general framework of "ordinary" photoionization, due to changes of the ionizing flux and mean photon energy in parts of the BLR.

Our observations are much more detailed than the ones used by Peterson and Ferland and can be used to clarify the situation. It is evident from our data that brightness changes of both He II lines are quite common (Fig. 12). It is also evident that the He II lines do not show any sign of a B component; thus the comparison with Hβ, which is dominated by the B component and does not show the VB component, is not meaningful. Moreover, we suspect that the Peterson and Ferland measurement of the He II λ4686 intensity, prior to the 1984 March event, may not be very accurate, because they were not aware of the completely different profile of this line. Our observations are good and cover most of this period, and we see no change of flux by a factor of 10, as claimed by them. The observational situation is in fact much simpler; a VB He II line that behaves much like the VB components of Lα and C IV λ1549 in response to continuum flux variations. The amplitude is large, up to factor of 4 or so, but there is no need to invoke new supply of material to explain this behavior. Our observations thus support the general picture suggested by Kallman and Elitzur (1988), although the situation is somewhat complicated by the fact that only the VB component is detected and responds to the continuum variations. We should also mention here that for the VB line component the line ratio He II λ1640/He II λ4686 is variable in the sense that it changes from about 10, when $F(1350)$ is low to about 4 when the continuum is high. This suggests strongly that these two pure recombination lines

may be differently influenced by the intensity of the ionizing continuum. In this case, recombination theory or even a more complete analysis as done by Netzer *et al.* (1985) might not be sufficient to interpret these lines. Reddening estimates based on such models for the region of the VB components may then easily be wrong.

Our observations of He I λ5876 are also consistent with it having only a VB component. There are observational and theoretical problems associated with that. First, the line fitting is complicated for this line. Secondly, it is difficult to understand a situation where a gas cloud is producing strong hydrogen lines but no neutral helium lines (i.e., the B component). This question must be further investigated.

The general picture that emerges from the study of the hydrogen and helium lines in NGC 5548 is that of a stratified gas distribution. Clouds closer in have the highest excitation and produce strong He II lines, some Lyα, and no detectable Balmer lines. The excitation further out is lower. There is hardly any He^{++}, but the Balmer lines are strong (B component). This picture is also consistent with the observations of all line components in C IV λ1549 and Mg II λ2798. The stratification in ionization appears to correspond to a stratification in velocity structure as shown in the various line components. Future line reverberation studies may provide the dimensions and physical conditions in these dynamically separated gas components.

VI. SUMMARY

We have presented the results of an extensive coordinated ultraviolet and optical spectroscopic study of the Seyfert 1 galaxy NGC 5548. A detailed continuum decomposition was made of the data, which cover the wavelength interval from 1150–7000 Å. The behavior of the variable continuum was established. The variable broad emission lines have been decomposed in a limited number of Gaussian components which could be identified as individually variable components in most lines. The following conclusions were reached on the detailed nature of the variability of NGC 5548:

a) Continuum

1. The continuum of NGC 5548 varies coherently from 1150 to 7000 Å (see Fig. 6).

2. The overall nonstellar continuum of NGC 5548 at 1150 Å $< \lambda <$ 7000 Å is well described by a power law; Balmer continuum; emission from the many blended broad Fe II lines (see Fig. 3).

3. The decrease in amplitude of the continuum variations at longer wavelengths can be fully accounted for by the contribution of the constant starlight in the aperture (see Figs 1, 2, and 6).

4. The independently variable part of the continuum can be fully described by a relatively flat power law ($F_\nu = \nu^{-\alpha}$, with $0.1 < \alpha < 0.5$) for 1150 Å $< \lambda <$ 7000 Å (see Fig. 3). The slope of this variable power law is slightly dependent on its brightness in the sense that the spectrum becomes harder when the AGN is brighter (eq. [1]).

5. The intensity in the semicontinuum formed by the Fe II lines is constant in the regions with $\lambda > 3000$ Å, while at shorter wavelength a small variability is present. The intensity in the Balmer continuum is a strong function of the UV-optical power-law continuum of the AGN. The best-defined Fe II blends in the optical are fully matched by the Fe II models used, convolved with a width of 4500 km s^{-1}, similar to the B component of Hβ. No evidence is found for the presence of a broad component to the [O III] lines at 5007 and 4959 Å.

b) Emission Lines

1. The emission lines were found to be separable in Gaussian components which are identifiably distinct in their response to continuum variations. With a line model consisting of four components and a narrow line, we have been able to reproduce all the major emission lines in the spectra Lyα, C IV λ1549, He II λ1640, C III] λ1909, Mg II λ2798, the Balmer lines, He II λ4686, and He I λ5876 (see Figs. 4 and 5 and Table 6) at many epochs.

2. Most of the narrow lines—defined to be unresolved at the resolution of our data (FWHM = 1400 km s^{-1} in the UV and 700 km s^{-1} in the optical)—do not show variability. The notable exception to this is the narrow Lyα line, which shows a strong decrease. This is suggested to be most likely a delayed response to the large continuum drop in 1981. In that case, the size of the NLR in NGC 5548 is 3 lt-yr (2.7×10^{18} cm). The lack of variation in the narrow C IV λ1549 presents some problems for such interpretation (see Fig. 10).

3. The line ratios in the NLR of NGC 5548 suggest that in the NLR of this Seyfert 1 galaxy the densities are higher (10^5–10^7 cm^{-3}) than those observed in Seyfert 2 galaxies such as NGC 3393 (see Table 3).

4. The He II ratio (λ1640/λ4686), thought to be a good indicator for reddening, was found to be 11.3 for the NLR. This value is considerably higher than predicted for the standard low-density conditions in the NLR and cannot easily be accommodated by the models.

5. All components in the broad lines are found to be variable, and these variations can in most cases be correlated to the continuum as measured through $F(1350)$.

6. Most of the flux in the broad lines is carried in two components. The broad line (B), which is at rest with respect to the narrow-line region and has a FWHM = 5000 km s^{-1}, and the very broad (VB) component at −2000 km s^{-1} and with a FWHM = 10,000 km s^{-1}. Two smaller components are found in some lines blue- and redshifted, respectively, from the systematic velocity by −2800 km s^{-1} and 2000 km s^{-1} (see Table 6).

7. The B component was identified in Lyα, C IV λ1549, C III] λ1909, Mg II λ2798, and the Balmer lines. The VB component is only present for Lyα, C IV λ1549, He λ1640, He II λ4686, and He I λ5876.

8. The Balmer decrement is a strong function of the continuum brightness measured at 1350 Å, and the variations are more pronounced for the higher members of the Balmer series. The Balmer continuum variations are as large as those shown by the Lyα line (see Fig. 13).

9. Although our data do not allow a detailed time delay study, some trends are indicated. The B components suggest a BLR smaller than 50 lt-day, while the VB components appear to respond faster than the B components. On the other hand, the B component of the Mg II λ2798 line does appear to respond with a delay of about 100 days, as do the Fe II(UV) blends. This suggests strongly the presence of stratification in the BLR.

10. The Lyα/C IV ratio increases with increasing continuum, contrary to the prediction from standard photoionization models. The C IV/C III] ratio remains constant over the continuum variations (see Fig. 14).

11. For the C IV (VB) components, the line strength increases with the continuum and reaches a maximum considerably

before the highest continuum level observed. For higher continuum fluxes, the line strength decreases again (see Fig. 11).

12. Both C IV and He II (VB) follow closely the variations of the continuum. The absence of the VB component in the Hβ line makes the "accretion event" identification for the He II line variations rather unnecessary (see Fig. 12).

13. The Balmer decrement is a strong function of the continuum brightness. This, together with the large amplitude in the Balmer continuum variations, suggests that the contribution of the VB gas to the Balmer continuum is considerable.

14. The very tight relations between the Balmer continuum and the Lyα line will allow the detailed continuum and line analysis applied to the combined data to also be applied at times when only UV data are available.

15. The variations seen in the ratio He II λ1640/He II λ4686 in the VB component suggest that, counter to expectations, this line ratio might not be such a good reddening indicator.

We would like to thank the European *IUEAC* for its continued and patient support for the Vilspa Observatory Program, under which many of the observations were made. We want to thank the present and past VILSPA staff members A. Cassatella, J. Clavel, C. Gry, C. Cacciari, P. Benvenuti, P. Patriarchi, and L. Bianchi. Without their professional dedication, such a program would have been impossible to accomplish.

APPENDIX

ERROR ANALYSIS

Since we are dealing with observations of a variable object, the determination of the accuracy of each measurement has to be related to quantities that can be derived internally from the individual spectra. For continuum measurements, one commonly uses the rms error $\sqrt{\Sigma(O-C)^2/(n-1)}$ measured over the window chosen to define the continuum. Since this represents the only objective measure available, we will relate the accuracy of each quantity to this value. All errors in this paper are derived from this value. For the nonstellar continuum, the Balmer continuum, and the Fe II blends, we assign the formal errors corresponding to the rms error in the chosen continuum windows. These errors are given in the tables and error bars are shown in the figures. Flux density errors in the 1350 Å continuum window are given in Tables 4 and 7. To be able to relate these rms internal errors to an actual error associated with a relative flux measurement in our time series, we compared the observed continuum for six epochs for which two separate SWP spectra were available, in several 50 Å windows over the range from 1200 to 1980 Å. The reproducibility of the results is about 3%, in agreement with the generally established repeatability of *IUE* data (Clavel, Gilmozzi, and Prieto 1988). Since the average rms error in our continuum fluxes at 1350 Å is 9%, this suggests that the errors we use correspond to 3 σ errors. Rather than dividing all errors by three, we have preferred to keep the errors as calculated directly, thus *all error bars in this paper are 3 σ errors.* The accuracy of the FES counts (Table 1) has been estimated to be approximately 6% from those dates on which independent measurements were made. For the optical data, we similarly used the rms error in the continuum window (Table 4). The final flux scale of the optical data was adjusted using the [O III] lines and did not introduce further uncertainties.

The Gaussian line fitting was done to a χ^2 minimization of 0.005, i.e., to the 99.5% confidence level, corresponding to a 3 σ determination. The errors in Table 6 for the FWHM and central positions are directly derived rms errors in the quantities from the final line fits. These errors only indicate the consistency of the fits starting from the standard profile. We derive the accuracy of the intensity measured in each component individually, directly from the results of the fitting procedure itself. First we evaluated the significance of the fits—i.e., assured that the information extracted from the data is consistent with the information content of the data—with a Kolmogorov test on the residuals. This was used to test for randomness in the Gaussian distribution of the residuals. The distribution was normalized to the rms residuals in the adjacent continuum windows. (This assumes implicitly that the signal-to-noise ratio in a single *IUE* spectrum is proportional to the intensity; since single *IUE* spectra are readout noise–limited, this is essentially correct.) For the stronger lines, we found the testing hypothesis to be correct at probabilities in excess of 30%, confirming the Gaussian distribution of the residuals of the fits and thus the statistical nature of the errors in the measured intensities of the components. The errors in the intensities of each line component were derived using the rms residuals over the part of the spectrum over which the line profile fit was made. The errors in the individual components were weighted with a "contrast factor," $W(i)/H(i)$, where $W(i)$ is the FWHM of the ith component in a line and $H(i)$ is the peak intensity of the ith component. The error in the intensity of each line component (i) is then given by

$$\epsilon(i) = [\text{rms (line)} \times W(i)/H(i)]/\sqrt{\Sigma[W(i)/H(i)]^2}\ . \tag{A1}$$

The application of equation (A1) retains the relation between the errors $\epsilon(i)$ of the individual line components and the error in the total line intensity: $[\text{rms(line)}]^2 = \Sigma[\epsilon(i)]^2$. The errors thus derived are given in Tables 7–12, and the figures show the corresponding error bars. Since the errors $\epsilon(i)$ are determined directly from the residuals of the line fits itself, and it has been shown above that these are equivalent to the continuum errors, the errors $\epsilon(i)$ correspond to approximately 3 σ errors. A comparison between the accuracy of the average FWHM in Table 6 and the errors derived using equation (A1) shows that they are fully consistent with the error definition of the component intensities of equation (A1).

An additional check of the validity of equation (A1) and the nature of our errors can be made through the comparison with the spread in the individually determined intensities of the nonvariable narrow-line component in e.g., Hβ and C IV λ1549. The formally weighted mean value (using eq. [A1]) of the narrow Hβ is 5.1 ± 0.1, and for C IV λ1549 it is 100 ± 2. The direct averaging of the results in Tables 8 and 11 gives 5.2 ± 0.4 for Hβ and 99.3 ± 1.8 for C IV λ1549 (units are 10^{-14} ergs s^{-1} cm^{-2}). This confirms that the 3 σ errors for the intensities of the fitted line components using equation (A1) are a good representation of the accuracy of the results.

REFERENCES

Alloin, D., Pelat, D., Phillips, M. M., and Whittle, M. 1985, *Ap. J.*, **288**, 205.
Atwood, B., Baldwin, J. A., and Carswell, R. F. 1982, *Ap. J.*, **257**, 559.
Barr, P., and Mushotzky, R. 1986, *Nature*, **320**, 421.
Barr, P., Willis, A. J., and Wilson, R. 1983, *M.N.R.A.S.*, **203**, 201.
Barylak, M., Wasatonic, R., and Imhoff, C. 1984, *ESA IUE Newsletter*, **20**, 55.
Boggess, A., *et al.* 1978, *Nature*, **275**, 2.
Bohlin, R. C., Holm, A. V., and Lindler, D. J. 1981, *ESA IUE Newsletter*, **10**, 10.
Branduardi-Raymont, G. 1988, in *IAU Symposium 134, Active Glactic Nuclei*, ed. D. E. Osterbrock and J. S. Miller (Dordrecht: Kluwer), p. 177.
Bromage, G. E., *et al.* 1985, *M.N.R.A.S.*, **215**, 1.
Burstein, D., and Heiles, C. 1982, *A.J.*, **87**, 1165.
Clavel, J., *et al.* 1987, *Ap. J.*, **321**, 251.
Clavel, J., Gilmozzi, R., and Prieto, A. 1988, *Astr. Ap.*, **191**, 392.
Clavel, J., and Wamsteker, W. 1987, *Ap. J. (Letters)*, **320**, L9.
Clavel, J., Wamsteker, W., and Glass, I. 1989, *Ap. J.*, **337**, 236.
Cohen, R. D. 1983, *Ap. J.*, **273**, 119.
Collin-Souffrin, S., Alloin, D., and Andrillat, Y. 1973, *Astr. Ap.*, **22**, 343.
Collin-Souffrin, S., Dumont, S., Joly, M., and Pequignot A. 1986, *Astr. Ap.*, **166**, 27.
Davidson, K., and Netzer, H. 1979, *Rev. Mod. Phys.*, **51**, 715.
de Bruyn, A., G. 1980, *Highlights Astr.*, **5**, 631.
Diaz, A. I., Prieto, M. A., and Wamsteker, W. 1988, *Astr. Ap.*, **195**, 53.
Elitzur, M. 1984, *Ap. J.*, **280**, 653.
Faelker, J., Gordon, F., and Sandford, M. C. W. 1987, in *Exploring the Universe with the IUE Satellite*, ed. Y. Kondo (Dordrecht: Reidel), p. 21.
Ferland, G. J. 1987, Internal Report, Ohio State University Astronomy Department 87-001.
Ferland, G. J., and Persson, S. E. 1989, preprint.
Foltz, C. B., Peterson, B. M., Capriotti, E. R., Byard, P. L., Bertram, R., and Lawrie, D. G. 1981, *Ap. J.*, **250**, 508.
Gilmozzi, R., *et al.* 1986, in *Physics of Formation of Fe* II *lines outside LTE*, ed. R. Viotti, A. Vittone, and M. Friedjung (Dordrecht: Reidel), p. 267.
Gregory, S., Ptak, R., and Stoner, R. 1982, *Ap. J.*, **261**, 30.
Holm, A. V., and Rice, G. 1981, *ESA IUE Newsletter*, **11**, 15.
Kallman, T., and Elitzur, M. 1988, *Ap. J.*, **328**, 523.
Kollatschny, W., Fricke, K. J., Schleicher, H., and Yorke, H. W. 1981, *Astr. Ap.*, **102**, L23.
Kwan, J., and Krolik, J. H. 1981, *Ap. J.*, **250**, 478.
Lyutyi, V. M. 1977, *Soviet Astr.*, **21**, 6.
Malkan, M. A., and Fillipenko, A. V. 1983, *Ap. J.*, **275**, 477.
McAlpine, G. M., Davidson, K., Gull, T. R., and Wu, C. C. 1985, *Ap. J.*, **294**, 147.
Netzer, H. 1987, *M.N.R.A.S.*, **225**, 55.
Netzer, H. 1989, *Comm. Ap.*, **14**, 137.
Netzer, H., and Davidson, K. 1979, *M.N.R.A.S.*, **187**, 871.
Netzer, H., Elitzur, M., and Ferland, G. J. 1985, *Ap. J.*, **299**, 752.
Netzer, H., *et al.* 1989, *IAU Circ.*, No. 4780.
Netzer, H., Wills, B. J., Wills, D., and Wamsteker, W. 1985, *Ap. J.*, **292**, 143.
Pelat, D., Alloin, D., and Fosbury, R. A. E. 1981, *M.N.R.A.S.*, **195**, 787.
Peterson, B. M. 1987*a*, *Ap. J.*, **312**, 79.
———. 1987*b*, in *IAU Symposium 121, Observational Evidence of Activity in Galaxies*, ed. E. Khachikian, G. Melnick, and K. Fricke (Dordrecht: Reidel), p. 161.
Peterson, B. M., and Ferland, G. J. 1986, *Nature*, **324**, 345.
Peterson, B. M., Foltz, C. B., Byard, P. L., and Wagner, M. R. 1982, *Ap. J. Suppl.*, **49**, 469.
Pounds, K. A., and Turner, T. J. 1988, *Mem. Soc. Astr. Italiana*, **59**, 261.
Puetter, R. C., and Hubbard, E. N. 1987, *Ap. J.*, **320**, 85.
Reimers, D., Clavel, J., Groote, D., Engels, D., Hagen, H. J., Naylor, T., Wamsteker, W., and Hopp, U. 1989, *Astr. Ap.*, **218**, 71.
Rodríguez-Pascual, P. M., Santos-Lleo, M., and Clavel, J. 1989, *Astr. Ap.*, **219**, 101.
Rodríguez-Pascal, P. M., Wamsteker, W., Netzer, H., and Wills, B. 1988, in *A Decade of UV Astronomy with the IUE Satellite*, ed. E. J. Rolfe (ESA SP-281), p. 311.
Seaton, M. J. 1979, *M.N.R.A.S.*, **187**, 73P.
Stripe, G. M., van Groningen, E., and de Bruyn, A. G. 1988, *Astr. Ap.*, **211**, 310.
Stoner, R., and Ptak, R. 1985, *Ap. J.*, **297**, 611.
———. 1984, *Ap. J.*, **280**, 516.
Ulrich, M. H., and Boisson, C. 1983, *Astr. Ap.*, **119**, 69.
Ulrich, M. H., *et al.* 1984, *M.N.R.A.S.*, **206**, 221.
Ulrich, M. H., Courvoisier, T. J. L., and Wamsteker, W. 1988, *Astr. Ap.*, **204**, 21.
van Groningen, E., and de Bruyn, A. G. 1988, *Astr. Ap.*, **211**, 293.
Veron-Cetty, M. P., Veron, P., and Tarenghi, M. 1983, *Astr. Ap.*, **119**, 69.
Wamsteker, W., Alloin, D., Pelat, D., and Gilmozzi, R. 1985, *Ap. J. (Letters)*, **295**, L33.
Wamsteker, W., and Barr, P. 1985, *Ap. J. (Letters)*, **292**, L45.
Wamsteker, W., and Colina, L. 1986, *Ap. J.*, **311**, 617.
Wamsteker, W., *et al.* 1984, in *Proc. 4th European IUE Conf.*, ed. E. J. Rolfe and B. Battrick (ESA SP-218), p. 97.
Wamsteker, W., *et al.* 1986, in *New Insights in Astrophysics*, ed. E. J. Rolfe (ESA SP-263), p. 701.
Wilkes, B. J., and Carswell, R. F. 1982, *M.N.R.A.S.*, **201**, 645.
Wills, B. J., Netzer, H., and Wills, D. 1985, *Ap. J.*, **288**, 94 (WNW).
Yee, H. K. C., and Oke, J. B. 1981, *Ap. J.*, **248**, 472.

M. Barylak, A. Talavera, and W. Wamsteker: ESA *IUE* Observatory, P.O. Box 50727, Madrid, 28080, Spain

P. Barr: Space Sciences Department, ESTEC, Astrophysics Division, Postbus 299, 2200 AG Noordwijk, Netherlands

R. Gilmozzi: Space Telescope Science Institute, Homewood Campus, Baltimore, MD 21218

A. Heck: C.D.S., Observatory Astronomique, 11 rue del'Universite, F–67000, Strasbourg, France

D. Maoz and H. Netzer: School of Physics and Astronomy and the Wise Observatory, Ramat Aviv, Tel Aviv 69978, Israel

P. Rodriguez-Pascual: Universidad Complutense, Madrid, Spain

Beverley J. Wills and D. Wills: Department of Astronomy, University of Texas, R.L.M. 15.308, Austin, TX 78712